Enhanced spin-mechanical interaction with levitated micromagnets

Xue-Feng Pan, Xin-Lei Hei, Xing-Liang Dong, Jia-Qiang Chen, Cai-Peng Shen, Hamad Ali, and Peng-Bo Li *

Ministry of Education Key Laboratory for Nonequilibrium Synthesis and Modulation of Condensed Matter,
Shaanxi Province Key Laboratory of Quantum Information and Quantum Optoelectronic Devices, School of Physics,
Xi'an Jiaotong University, Xi'an 710049, China

Spin-mechanical hybrid systems have been widely used in quantum information processing. However, the spin-mechanical interaction is generally weak, making it a critical challenge to enhance the spin-mechanical interaction into the strong coupling or even ultrastrong coupling regime. Here, we propose a protocol that can significantly enhance the spin-mechanical coupling strength with a diamond spin vacancy and a levitated micromagnet. A driving electrical current is used to modulate the mechanical motion of the levitated micromagnet, which induces a two-phonon drive and can exponentially enhance the spin-phonon and phonon-medicated spin-spin coupling strengths. Furthermore, a high-fidelity Schrödinger cat state and an unconventional two-qubit geometric phase gate with high fidelity and faster gate speed can be achieved using this hybrid system. This protocol provides a promising platform for quantum information processing with nitrogen-vacancy spins coupled to levitated micromagnets.

I. INTRODUCTION

Hybrid quantum systems, which combine the advantages of various quantum systems to overcome their shortcomings, have been widely used in quantum information processing [1–3]. Several proposals for hybrid systems in cavity quantum electrodynamics (QED) [4], circuit QED [5], and spin-mechanical hybrid systems [6–31] have already been implemented in recent years. The spin-mechanical hybrid system combines quantum systems with long coherence time, such as trapped atoms or ions [32–35], solid-state spins [36–42], and mechanical oscillators, with high-quality factors, such as cantilevers [17–24], nanobeams [12–15], and a nonlinear period-driven nanoelectromechanical oscillator [43]. It has been widely used in the preparation of a nonclassical quantum state of mechanical motion [25,26], ground-state cooling [15–17], ultrasensitive sensing [11,44], as well as the generation of interaction between two distant quantum systems [18–21]. The greatest impediment to its possible applications is the unavoidable dissipation of the oscillators interacting with the environment. To reduce dissipation, researchers have developed levitated devices [45–76] that readily isolated the oscillators from the environment.

Optical, electrical, and magnetic levitation are the three types of suspending setups that can all work in a vacuum environment. The magnetic trap with a passive field [45–54, 57–62] is simpler than the optical trap with lasers [63–66] and the electrical trap with radio-frequency modulation of a high-voltage electric field [33–35,56]. Photon recoil, damage to suspended particles due to absorption resulting in internal heating, and clamping losses can all be avoided via magneto-static field levitation [62,76]. For these suspended schemes, the suspension objectives are diverse. Glass spheres [65], superconductor spheres [68,74], superconductor rings [48,73], magnetic microspheres [44,45], silicon particles [64,70], and diamond particles [58–63] have all been investigated on various platforms. Because of their isolation, they have been used to construct ultrasensitive sensors [44,45] as well as to couple superconducting circuits [54–57,73,73] and solid-state spins [16,35,70]. Magnetic microspheres, particularly yttrium iron garnet (YIG) spheres due to their high spin density [77], have received a great attention [78–86]. There have been investigations on magnon coupling to cavity modes such as sphere cavity [81], coaxis cavity [82], three-dimensional (3D) cavity [83], and so on. Classical Rabi-like oscillation [84], magnetically induced transparency [84], bistable states [85], and other intriguing quantum effects have been observed. Furthermore, the YIG sphere can couple to microwave photons and solid-state spins [86,87], which has been utilized to improve the coupling strength between a solid-state spin and a photon mode [86]. Also, the coupling of a one-dimensional chiral spin ring and a bosonic magnon reservoir was studied in Ref. [88], proving that controlling the direction of information flow can be achieved by controlling the applied external field. In addition, levitated micromagnets coupled to solid-state spins have been studied [52]. A recent study has showed the interaction of a nitrogen-vacancy (NV) center in diamond with a levitated micromagnet through the magnetic field gradient produced by the micromagnet [52]. The coupling strength, however, is so weak that it cannot be used for quantum information tasks.

Inspired from previous experimental and theoretical progress, we propose a useful approach to exponentially enhance the spin-mechanical coupling strength in a spin-magnetomechanical system. An NV center is situated near the

---

*lipengbo@mail.xjtu.edu.cn

hard spherical micromagnet, which levitates above the type-II superconductor. The magnetic field gradient generated by the micromagnet couples the NV center to the center-of-mass motion of the micromagnet. Many schemes have been proposed to enhance the single-quantum interaction on various platforms. Nonlinear resources [89–92] and parametric drive [93,94] (for example, two-photon drive) have been utilized to increase light-matter interactions. The modulation of voltage in a trapped-ion system is used to achieve parametric amplification [95–97]. Modulating the spring constant of a cantilever [98] increases the spin-phonon coupling strength exponentially in a spin-mechanical system [20]. This work suggests a classical electrical-current-driven approach for achieving exponential enhancement of spin-mechanical interactions in a suspended micromagnet platform. The driving current is located above the levitated micromagnet. The trap potential is modified by the magnetic field of the current, which modulates the oscillation frequency of the micromagnet's mechanical motion. This modulation process can provide a two-phonon drive capable of amplifying the mechanical zero-point fluctuations, hence increasing the spin-mechanical interaction. In other words, despite merely employing a classical drive current, we obtain a nonlinear resource and, as a consequence, achieve the strong coupling regime without adding any nonlinear sources into the system. Utilizing the strongly coupled spin-mechanical system, one can prepare a high-fidelity superposition state of the levitated micromagnet. In addition, phonon-mediated spin-spin coupling can be obtained when two NV centers are coupled to the same mechanical oscillator [18–21], and the interaction can also be exponentially amplified with a driving current. With the enhanced spin-spin coupling, the two-NV protocol can also construct an unconventional two-qubit geometric phase gate with the property of high fidelity, shorter operation time, and universality.

II. SETUP AND PROTOCOL

A. The setup

Figure 1(a) presents a hybrid system that includes a micromagnet, an NV center, and a driving current. The hard spherical micromagnet with radius a and mass m levitates on the type-II superconductor because of the flux trapping effect, the superconductor freezing or trapping the magnetic flux that penetrates it during the cooldown [see Fig. 1(a)] [52,69,99]. The microfabricated pocket provides a stable vacuum environment to isolate the micromagnet from the environment, enabling the dissipation of the system to be decreased. A cosine-function drive is provided by the current above the micromagnet, and the NV center is placed nearby the micromagnet. Figure 1(b) depicts the principle of this setup. The micromagnet trapped in the magnetostatic field, which can be calculated via the frozen dipole model [Fig. 1(c)], can be compared to a simple harmonic oscillator that couples to the NV center. The NV center transition [Fig. 1(d)] is driven by a linearly polarized microwave in the y direction, and the transverse static magnetic field [i.e., x direction] results in a mix of the eigenstates of $\hat{\sigma}_z$. The energy level structure of the mixed states is depicted in Fig. 1(e). Figure 1(f) presents
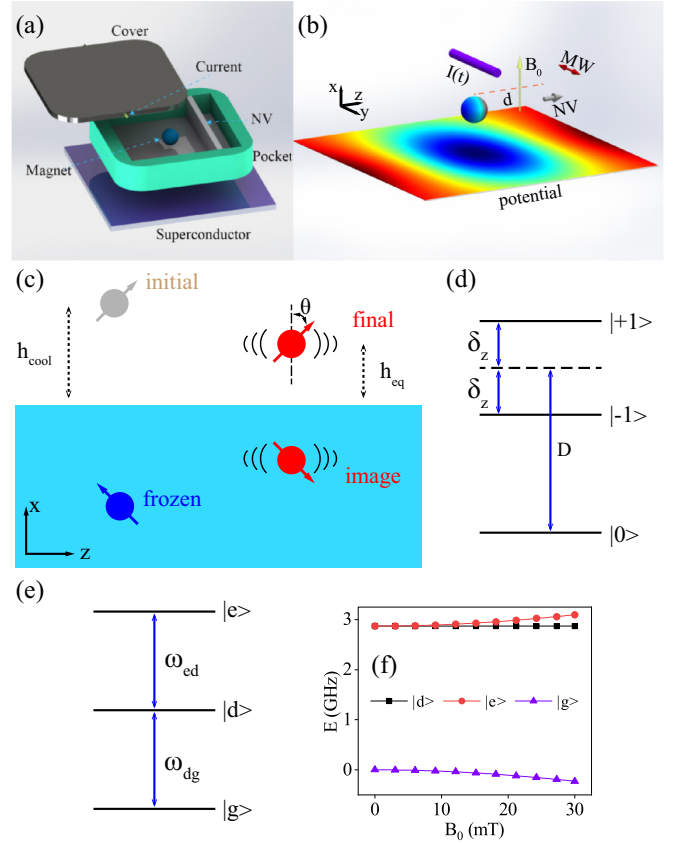

FIG. 1. Setup sketch: (a) The model of our proposal. (b) The principle of our setup. (c) The frozen dipole model. (d) The energy level structure of NV centers. It will produce Zeeman splitting when a z-direction magnetic field is applied. (e) The energy level structure of the mixed states. (f) The energy level splitting of the mixed states varies with the x-direction magnetic field.

the energy level splitting of the mixed states varying with the x-direction magnetic field.

B. Levitation of the micromagnet

As shown in Fig. 1(b), the position of the levitated micromagnet with mass m and radius a in the direction of gravity is represented by x. The acceleration of gravity is $g = 9.8 \text{ m/s}^2$. The position vectors of frozen and image dipoles are $\boldsymbol{R}_f = (-h_{\text{cool}}, 0, 0)$ and $\boldsymbol{R}_i = (-x, y, z)$ with cooldown height h_{cool}, respectively. The orientation corresponds to $\boldsymbol{\mu}_f = \mu_m(\cos\theta_{\text{cool}}, 0, -\sin\theta_{\text{cool}})$ and $\boldsymbol{\mu}_i = \mu_m(-\cos\theta, \sin\theta\sin\phi, \sin\theta\cos\phi)$ with dipole moment μ_m, respectively. The position vector and magnetic moment of the micromagnet are $\boldsymbol{\mu}_l = \mu_m(\cos\theta, \sin\theta\sin\phi, \sin\theta\cos\phi)$ and $\boldsymbol{R}_l = (x, y, z)$, respectively. The magnetic field produced by a dipole $\boldsymbol{\mu}$ at a position $\boldsymbol{r}$ is given by

$$\boldsymbol{B} = \frac{\mu_0}{4\pi}\left(\frac{3\boldsymbol{r}(\boldsymbol{\mu}\cdot\boldsymbol{r})}{r^5} - \frac{\boldsymbol{\mu}}{r^3}\right). \qquad (1)$$

According to the frozen dipole model [99], the effective magnetic field $\boldsymbol{B}_{\text{eff}}$ at the position of the levitated micromagnet consists of the magnetic field $\boldsymbol{B}_f$ generated by a frozen dipole and the magnetic field $\boldsymbol{B}_i$ generated by an image dipole, as
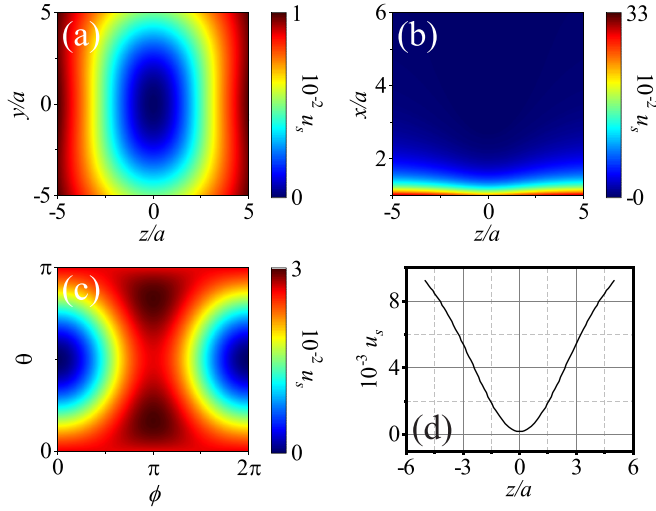
FIG. 2. The potential energy of the levitated micromagnet. The dimensionless potential energy u_s in the zy plane, zx plane, $\theta\phi$ plane, and z direction are shown in (a), (b), (c), and (d), respectively. Here, the radius and the density of the micromagnet are $a = 22.4\ \mu$m and $\rho = 7430$ kg/m^3, respectively. The initial position and the equilibrium position are both $3a$, the initial orientation is $\phi_{cool} = 0$ and $\theta_{cool} = \pi/2$, and the residual induction is $B_r = 750$ mT.

depicted in Fig. 1(c). Then the potential energy of the levitated micromagnet is given by

$$U = -\boldsymbol{\mu} \cdot \boldsymbol{B}_{\text{eff}} + mgx, \quad (2)$$

where $\boldsymbol{B}_{\text{eff}} = \boldsymbol{B}_f + 1/2\boldsymbol{B}_i$ is the effective magnetic field produced by the interaction between the micromagnet and type-II superconductor [52]. We can derive an analytic formula for the potential energy U as

$$U = U_s u_s, \quad (3)$$

with

$$
\begin{aligned}
u_s &= \alpha_s x_s + g_u, \\
g_u &= \frac{3 + \cos 2\theta}{6x_s^3} \\
&\quad - \frac{16}{3} \frac{g_c \cos\theta + g_s \sin\theta}{\left[(x_s + h_{cool})^2 + y_s^2 + z_s^2\right]^{5/2}}, \\
g_c &= \left[2(x_s + h_{cool})^2 - y_s^2 - z_s^2\right] \cos\theta_{cool} \\
&\quad - 3z_s(x_s + h_{cool}) \sin\theta_{cool}, \\
g_s &= 3(x_s + h_{cool})(y_s \sin\phi + z_s \cos\phi) \cos\theta_{cool} \\
&\quad + \left\{\left[(x_s + h_{cool})^2 + y_s^2 - 2z_s^2\right] \cos\phi - 3z_s y_s \sin\phi\right\} \\
&\quad \times \sin\theta_{cool},
\end{aligned}
\quad (4)
$$

where $l_s = l/a$ ($l = x, y, z$, radius a as characteristic length scale), $\alpha_s = a/\alpha_{crit}$, $U_s = mg\alpha_{crit}$, and $\alpha_{crit} = B_r^2/(16g\rho\mu_0)$. B_r, ρ, and μ_0 are residual induction, density of the micromagnet, and vacuum permeability, respectively. The dimensionless potential energy defined by $u_s = \alpha_s x_s + g_u$ in Eq. (3) is plotted in Fig. 2, showing that the micromagnet can be steadily trapped in the potential trap. Figures 2(a), 2(b), and 2(c) present the dimensionless potential energy u_s of the micro-

magnet in the zy plane, zx plane, and $\theta\phi$ plane, respectively. In the zy direction, the potential energy exhibits strong symmetry. The equilibrium position of the levitation micromagnet is $(x_{eq}, y_{eq}, z_{eq}, \theta_{eq}, \phi_{eq}) = (h_{eq}, 0, 0, \pi/2, 0)$, where h_{eq} is the location of the minimum value of the potential energy in the direction of gravity. The potential energy distribution along the z axis illustrated in Fig. 2(d) can be well approximated as a harmonic potential, implying that the motion of the micromagnet is harmonic. The potential energy along the z direction can be denoted by

$$U = U_s \left\{\frac{16}{3} \frac{2z^2 - (h_{eq} + h_{cool})^2}{[(h_{eq} + h_{cool})^2 + z^2]^{5/2}} + \frac{1}{3h_{eq}^3} + \alpha_s h_{eq}\right\}, \quad (5)$$

where h_{eq} and h_{cool} correspond to the equilibrium position and the cooling height, respectively. We assign $\phi = \phi_{eq} = 0$ and $\theta = \theta_{eq} = \pi/2$. This indicates that the rotation of the micromagnet is neglected. Because the frequency of the rotation mode is much larger than the frequency of the translational mode, the interaction between the rotation mode and the NV center can be ignored according to the big detuning condition. By expanding at the equilibrium position and removing the constant and high-order components, the potential energy can be written as simple harmonic potential

$$U = \tfrac{1}{2} k_{ma} z^2, \quad (6)$$

where

$$k_{ma} = \frac{\mu_0 \mu_m^2}{4\pi} \frac{3}{(h_{eq} + h_{cool})^5}. \quad (7)$$

The motion of the levitated micromagnet along the z direction can be regarded as a simple harmonic motion, as represented by

$$\hat{H}_{ma} = \frac{\hat{p}^2}{2m} + \frac{1}{2} k_{ma} \hat{z}^2, \quad (8)$$

where $\hat{p}_z$ and $\hat{z}$ are momentum and position operators, respectively. By quantizing the Hamiltonian with $\hat{p}_z = -i\sqrt{m\omega_{ma}/2}(\hat{a} - \hat{a}^\dagger)$, $\hat{z} = z_0(\hat{a} + \hat{a}^\dagger)$, and $z_0 = \sqrt{1/(2m\omega_{ma})}$, we can obtain

$$\hat{H}_{ma} = \omega_{ma}\hat{a}^\dagger\hat{a}, \quad (9)$$

where $\omega_{ma} = \sqrt{k_{ma}/m}$ represents the trapping frequency associated with the cooling conditions, and $\hat{a}$ ($\hat{a}^\dagger$) represents the annihilation (creation) operator.

C. Hamiltonian of the system

The NV center is coupled to the micromagnet in this protocol through the magnetic field gradient induced by the micromagnet in the z direction. In the presence of a homogeneous static magnetic field in the x direction $\boldsymbol{B}_s = B_0\hat{\boldsymbol{e}}_x$, the ground state Hamiltonian of the NV center can be written as $\hat{H}_{NV} = D\hat{S}_z^2 + \gamma_e\hat{\boldsymbol{S}} \cdot \boldsymbol{B}_s$, where $\gamma_e = g_e\mu_B$ is the electron gyromagnetic factor and $D/2\pi = 2.87$ GHz is the zero-field splitting between sublevel $|m_s = 0\rangle$ and $|m_s = \pm 1\rangle$ [see Fig. 1(d)]. $g_e \simeq 2$ and $\mu_B = 14$ MHz/mT are the Landau factor of electron and Bohr magneton, respectively. $\hat{\boldsymbol{S}}$ is the electron spin operator including the components $\hat{S}_x$, $\hat{S}_y$, and $\hat{S}_z$. The microwave (MW) drive $B_y(t) = B_y^0 \cos(\omega_p t)$ polarized

in the y direction is applied to drive the transition between the sublevels, where B_y^0 and ω_p are the amplitude and frequency of the microwave drive, respectively. Then the Hamiltonian is given by

$$\hat{H}_{\mathrm{NV}} = D\hat{S}_z^2 + \delta\hat{S}_x + \Omega_p \cos(\omega_p t)\hat{S}_y, \quad (10)$$

where $\Omega_p = \gamma_e B_y^0$ is the Rabi frequency and $\delta = \gamma_e B_0$.

The interaction between the NV center and the micromagnet will be the subject of our next discussion. Here we neglect the coupling between the rotation of the micromagnet and the NV center, and only consider the coupling between the oscillation in the z direction and the NV center. The interaction between the other freedom degrees and the NV center is discussed in detail in Appendix B. The micromagnet can be described as a magnetic dipole in classical electrodynamics, with Eq. (1) describing the magnetic field surrounding it. Only the magnetic field in the z direction at position $(h_{\mathrm{eq}}, 0, d)$ of the NV center is concerned here, which is given by $\boldsymbol{B} = 2\mu_0\mu_m\hat{\boldsymbol{e}}_z/[4\pi(d-z)^3]$. For magnetic fields in other directions, when the position of the NV center is strictly located at $x = 0$ and $y = 0$, only the magnetic field in the z direction exists ($B_x = B_y = 0$, $B_z = 289$ mT); when there is an error of 10 nm for the position of the NV center, the maximum value of the magnetic field in the x and y directions is 7 mT, while the minimum value of the magnetic field in the z direction is 288 mT, i.e., $B_x, B_y \ll B_z$. Then we can ignore the effect of the magnetic field in the xy direction. The magnetic field is represented by

$$\boldsymbol{B} \simeq \frac{2\mu_0\mu_m\hat{\boldsymbol{e}}_z}{4\pi d^3} + \frac{6\mu_0\mu_m\hat{z}\hat{\boldsymbol{e}}_z}{4\pi d^4} + O(\hat{z}^2) \quad (11)$$

around the equilibrium position. After removing the high-order and constant components, and quantizing the motion, the interaction Hamiltonian is expressed as

$$\hat{H}_{\mathrm{int}} = \gamma_e \boldsymbol{B} \cdot \boldsymbol{S} = \lambda(\hat{a} + \hat{a}^\dagger)\hat{S}_z, \quad (12)$$

where $\lambda = 2\gamma_e B_r a^3 z_0/d^4$ is the coupling strength, d is the distance between the NV center and the micromagnet, and z_0 is the zero-point fluctuation.

Finally, $I_{\mathrm{cu}} = I_0 \cos(2\omega_{\mathrm{cu}}t)$ is the drive current placed above the micromagnet, where ω_{cu} is the driving current frequency and I_0 is the amplitude of the driven electrical current. The Hamiltonian of the driving current is given by $\hat{H}_{\mathrm{cu}} = 1/2k_{\mathrm{cu}}^2\hat{z}^2\cos(2\omega_{\mathrm{cu}}t)$. After quantization (Appendix C), we can have

$$\hat{H}_{\mathrm{cu}} = -g_{\mathrm{cu}}(\hat{a} + \hat{a}^\dagger)^2 \cos(2\omega_{\mathrm{cu}}t), \quad (13)$$

where $g_{\mathrm{cu}} = k_{\mathrm{cu}}z_0^2/2$ defines the coupling strength between the driving current and the micromagnet. The nonlinear term or the parametric amplification is obtained by the linear drive. The spin-mechanical coupling strength can be exponentially enhanced with such a nonlinear term, as demonstrated below. The drive current will inevitably have an effect on the NV center, and the influence of the magnetic field induced by it on the NV center is discussed in detail in Appendix C. Through calculation and analysis, it can be proved that the effect of driving current on the NV center is negligible in our model.
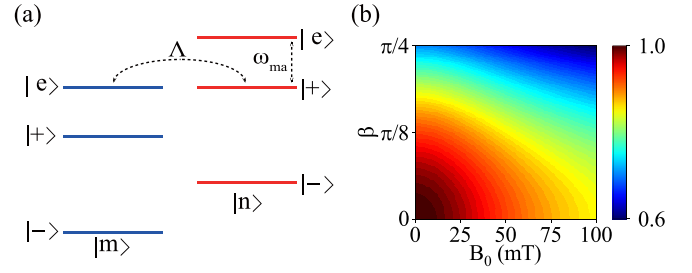

FIG. 3. Spin-phonon coupling. (a) Couplings between the spin and phonons. (b) The intensity of the spin-phonon coupling as a function of β and the transverse static magnetic field B_0.

III. ENHANCING THE COUPLING STRENGTH

A. One NV

Based on the foregoing analysis, the total Hamiltonian of the hybrid system is

$$\hat{H}_{\mathrm{TO}} = \hat{H}_{\mathrm{NV}} + \hat{H}_{\mathrm{ma}} + \hat{H}_{\mathrm{int}} + \hat{H}_{\mathrm{cu}}. \quad (14)$$

The first term is the Hamiltonian of NV centers. The second corresponds to the free Hamiltonian of the micromagnet, the third describes the interaction between the NV center and micromagnet, and the last is the drive-current Hamiltonian. In the absence of the microwave drive, the Hamiltonian $\hat{H}_{\mathrm{NV}}$ is given by

$$\hat{H}_{\mathrm{NV}} = D\hat{S}_z^2 + \delta\hat{S}_x. \quad (15)$$

The eigenstates of Eq. (15) are mixed states $|e\rangle = \sin\theta|0\rangle + \cos\theta|b\rangle$, $|g\rangle = \cos\theta|0\rangle - \sin\theta|b\rangle$, and $|d\rangle = (|+1\rangle - |-1\rangle)/\sqrt{2}$, where $|b\rangle = (|-1\rangle + |+1\rangle)/\sqrt{2}$ and $\tan 2\theta = 2\delta/D$, corresponding to the eigenenergy $\omega_{e/g} = D[1 \pm \sqrt{1 + (2\delta/D)^2}]/2$, and $\omega_d = D$.

We assume that the microwave is solely used to drive the transition between the mixed states $|g\rangle$ and $|d\rangle$, i.e., $\omega_p \simeq \omega_d - \omega_g = \omega_{dg}$. Transforming to the frame at the microwave frequency and using the rotating-wave approximation, the Hamiltonian in the basis $|e, d, g\rangle$ of the NV center can be reduced as

$$\hat{H}_{\mathrm{NV}} = \begin{pmatrix} -\frac{\Delta}{2} & 0 & 0 \\ 0 & \frac{\Delta}{2} & 0 \\ 0 & 0 & \omega_e'' \end{pmatrix} + \frac{1}{2i}\begin{pmatrix} 0 & -\Omega_p' & 0 \\ \Omega_p' & 0 & 0 \\ 0 & 0 & 0 \end{pmatrix}, \quad (16)$$

where $\Delta = \omega_p - \omega_{dg}$, $\omega_e'' = \omega_e - (\omega_d + \omega_g + \omega_p)/2$, and $\Omega_p' = \Omega_p \cos\theta$. We consider a basis for further diagonalization consisting of the eigenstates of Eq. (16), which are $|e\rangle$, $|+\rangle = i\sin\beta|g\rangle + \cos\beta|d\rangle$, and $|-\rangle = -i\cos\beta|g\rangle + \sin\beta|d\rangle$, with eigenenergies ω_e'' and $\omega_\pm = \pm\sqrt{\Delta^2 + \Omega_p'^2}/2$, where $\tan 2\beta = \Omega_p'/\Delta$. Here we consider energy levels $|e\rangle$ and $|+\rangle$ as a qubit with resonance frequency defined as $\omega_0 \equiv \omega_e'' - \omega_+$, and we take into account the resonance condition $\omega_0 \approx \omega_{\mathrm{ma}}$, as shown in Fig. 3(a). Using the eigenbasis $|e, \pm\rangle$ and the unitary transformation $U = \exp(-i\hat{H}_u t)$ with $\hat{H}_u = \omega_{\mathrm{cu}}(\hat{\sigma}_z/2 + \hat{a}^\dagger\hat{a})$ and rotating wave approximation, the Hamiltonian of the hybrid system is represented as

$$\hat{H}_{\mathrm{TO}} = \frac{\delta_0}{2}\hat{\sigma}_z + \delta_m\hat{a}^\dagger\hat{a} + \Lambda(\hat{a}\hat{\sigma}^+ + \hat{a}^\dagger\hat{\sigma}^-) - \frac{g_{\mathrm{cu}}}{2}(\hat{a}^2 + \hat{a}^{\dagger 2}), \quad (17)$$
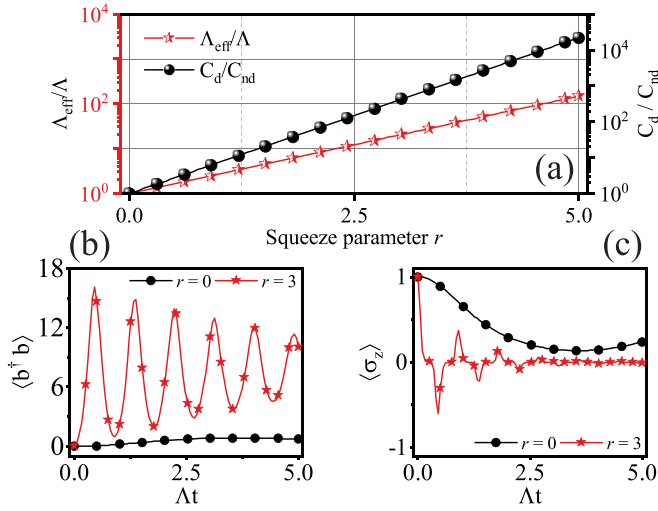
FIG. 4. Spin-phonon coupling. (a) $\Lambda_{\text{eff}}/\Lambda$ and C_d/C_{nd} as a function of the squeezing parameter r. The spin-phonon coupling strength appears to be enhanced exponentially. (b and c) The dynamic processes with ($r = 3$) and without ($r = 0$) the drive current, respectively. Here the initial state is $|0\rangle|\uparrow\rangle$, where the $|\uparrow\rangle$ represents the excited state $|e\rangle$. The coefficients are $\delta_m = \Lambda$, $\delta_0 = 0$, and $r = 0, 3$. The dephasing of NV centers and the dissipation of the micromagnet are $\gamma_{\text{NV}} = 0.1\Lambda$ and $\kappa_{\text{ma}}^S = 0.1\Lambda$, respectively.

where $\hat{\sigma}_z \equiv |e\rangle\langle e| - |+\rangle\langle +|$, $\hat{\sigma}_x = \hat{\sigma}^+ + \hat{\sigma}^-$, $\hat{\sigma}^+ \equiv |e\rangle\langle +|$, $\hat{\sigma}^- \equiv |+\rangle\langle e|$, $\delta_0 = \omega_0 - \omega_{\text{cu}}$, and $\delta_m = \omega_{\text{ma}} - \omega_{\text{cu}}$. Here only the states $|m, +\rangle$ and $|n, e\rangle$ are resonant with the condition $n = m + 1$, with m and n being the phonon numbers [see Fig. 3(a)]. Under the aforesaid resonant condition, the spin-phonon coupling strength is given by $\Lambda = \lambda \cos\theta \cos\beta$, which is related to the transverse magnetic field B_0 and β, depending on Ω_p' and Δ, as shown in Fig. 3(b). The coupling strength increases as B_0 and β decrease, showing that we should choose an appropriate value to make the system work well.

Using the Bogoliubov transformation [93,97,100] $\hat{b} = \hat{a} \cosh r - \hat{a}^\dagger \sinh r$, with $\tanh(2r) = g_{\text{cu}}/\delta_m$, the total Hamiltonian can be expressed in a simple form

$$\hat{H}_{\text{TO}} = \hat{H}_{\text{RO}} + \hat{H}_{\text{Sq}}, \tag{18}$$

$$\hat{H}_{\text{RO}} = \frac{\delta_0}{2}\hat{\sigma}_z + \Delta_m \hat{b}^\dagger \hat{b} + \Lambda_{\text{eff}}(\hat{b} + \hat{b}^\dagger)\hat{\sigma}_x, \tag{19}$$

$$\hat{H}_{\text{Sq}} = \frac{\Lambda e^{-r}}{2}(\hat{b} - \hat{b}^\dagger)(\hat{\sigma}^+ - \hat{\sigma}^-), \tag{20}$$

where $\Lambda_{\text{eff}} = \Lambda e^r/2$ and $\Delta_m = \delta_m/\cosh(2r)$. $\hat{b}$ ($\hat{b}^\dagger$) is the annihilation (creation) operator of Bogoliubov modes. Because of the driving current, the spin-phonon coupling strength can be enhanced exponentially. The spin-phonon coupling strength is orders of magnitude larger than the original one, as seen in Fig. 4(a). Because the item e^{-r} decreases to zero as the squeezing parameter r increases, the term $\hat{H}_{\text{Sq}}$ can be ignored.

To quantify the spin-mechanical coupling strength the cooperativity $C_{\text{nd}} = \Lambda^2/(\kappa_{\text{ma}}\gamma_{\text{NV}})$, a dimensionless parameter, is introduced, where κ_{ma} and γ_{NV} are the mechanical dissipation and the spin dephasing, respectively. Inevitably, as the coupling strength is amplified, so is the mechanical noise.

To alleviate the negative consequences of amplified mechanical noise, the dissipative squeezed scheme proposed in the literature [20,101,102] can be used. We consider that the micromagnetic sphere can couple with an additional optical mode or cavity mode with a two-tone drive. When the dissipation of the additional mode is large, an effective phonon dissipation κ_{ma}^S is induced, which cools the phonon mode to the ground state. Through the dissipative squeezed method, the b mode is always in the ground state in the squeezed picture. In this case, the Lindblad master equation of the system can be expressed as

$$\dot{\hat{\rho}} = -i[\hat{H}_{\text{RO}}, \hat{\rho}] + \kappa_{\text{ma}}^S D(\hat{b})\hat{\rho} + \gamma_{\text{NV}} D(\hat{\sigma}_z)\hat{\rho}, \tag{21}$$

where $D(\hat{O})\hat{\rho} = \hat{O}\hat{\rho}\hat{O}^\dagger - \{\hat{O}^\dagger\hat{O}, \hat{\rho}\}/2$ is the Lindblad operator, and κ_{ma}^S is the effective mechanical dissipation resulting from the interaction between the mechanical mode and the auxiliary bath. And then effective cooperativity with the driving current is given by $C_d = \Lambda_{\text{eff}}^2/(\kappa_{\text{ma}}^S \gamma_{\text{NV}})$. As a result, we can get $C_d/C_{\text{nd}} \sim e^{2r}$, which is magnified exponentially, as shown in Fig. 4(a). Using the master equation (21), we numerically evaluate the dynamic processes with and without the driving current. In the absence of the driving current, the coupling strength between spins and phonons is extremely weak, resulting in no Rabi oscillation; in the presence of the driving current, the spin-phonon coupling strength is greatly enhanced, resulting in Rabi oscillations, as illustrated in Figs. 4(b) and 4(c). To put it in other words, the driving current can be employed to enhance the spin-phonon coupling.

B. Geometric phase

Now we focus on the process of enhancement in phase space. Considering Eq. (19), for the sake of simplicity, we set $\delta_0 = 0$ and move into the Bogoliubov-mode interaction representation. The time evolution operator of the system $U_{\text{RO}}(t) = D[\alpha(t)]\exp[i\Phi(t)\hat{\sigma}_x^2]$ is obtained via Magnus expansion [103–106], where $D[\alpha(t)] = \exp[\alpha(t)\hat{b}^\dagger - \alpha^*(t)\hat{b}]\hat{\sigma}_x$ is the displacement operator and $\alpha(t) = \Lambda_{\text{eff}}/\Delta_m(1 - e^{i\Delta_m t})$ is the coherent displacement of the phonon in phase space. The spin and phonon are decoupled at time $t = 2\pi N/\Delta_m$ with $N = 1, 2, 3, \ldots$, as shown by the time evolution operator $U_{\text{RO}}(t)$, and the phonon returns to its initial state. In Fig. 5(a), the phonon-mode trajectory is shown in phase space. Due to the driving current, the phase space trajectory is magnified and covers a broader area. In addition, the phonon migration direction in phase space is correlated to the spin state, as indicated in equation $D[\alpha(t)]$. Under the original representation, i.e., the interaction representation of phonons, the phase space displacement of phonons is written as $\alpha_I(t) = \Lambda/(2\Delta_m)[(\cos\Delta_m t - 1)e^{2r} - i\sin\Delta_m t]$ [95,97].

The geometric phase Φ is determined only by the enclosed area swept away by phonon trajectories in phase space, as given by

$$\Phi = Im\left[\int_0^t \alpha^*(t')\,d\alpha(t')\right]. \tag{22}$$

The geometric phase with the driving current at time $t = 2\pi/\Delta_m$ (phonons orbit once in phase space) is given by $\Phi_d = 2\pi(\Lambda_{\text{eff}}/\Delta_m)^2$. In Fig. 5(b), $\Phi_d/\Phi_{\text{nd}} \propto (e^r \cos 2r)^2$ is
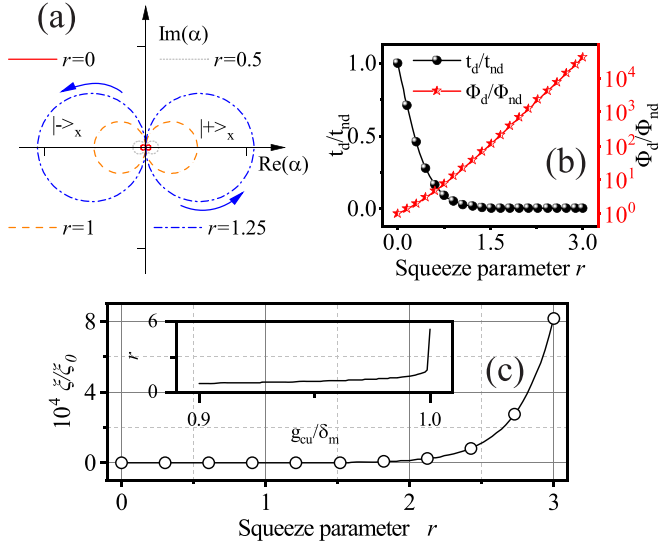
FIG. 5. (a) Phonon trajectory in phase space, which encloses a larger area as the squeeze parameter increases. (b) Geometric phase (in one period) and time (required to acquire a given geometric phase) as a function of the squeezing parameter r. (c) The phonon-mediated spin-spin coupling strength varies with the squeezing parameter r. The squeezing parameter r is plotted as a function of the ratio g_{cu}/δ_m in the inset.

shown as a function of the squeezing parameter r, where $\Phi_{nd} = 2\pi (\Lambda/\delta_m)^2$ is the geometric phase sans drive. The geometric phase is roughly exponentially increased. We currently consider acquiring a certain geometric phase Φ_0. After that, we can get $t_d/t_{nd} \propto 1/(e^r \cosh 2r)$, where t_d and t_{nd} are the time required to acquire Φ_0 with and without a drive, respectively. As seen in Fig. 5(b), increasing the squeezing parameter r reduces the time required to acquire a given phase Φ_0.

C. Two NVs

We now discuss the interaction of two NV centers with a micromagnet. Two NVs are symmetrically arranged on either side of the micromagnet along the magnetic field direction, coupling to the micromagnet center of mass motion via a strong magnetic field gradient. Two NV centers are symmetrically placed at positions $(h_{eq}, 0, d)$ and $(h_{eq}, 0, -d)$ on either side of the micromagnet along the direction of magnetization. Along the z axis, the magnetic field produced by the micromagnet is given by

$$\boldsymbol{B_1} = \frac{\mu_0 \mu_m}{2\pi (d-z)^3} \hat{\boldsymbol{e}}_z, \tag{23a}$$

$$\boldsymbol{B_2} = \frac{\mu_0 \mu_m}{2\pi (d+z)^3} \hat{\boldsymbol{e}}_z. \tag{23b}$$

After expanding at the equilibrium position, omitting constant items and high-order components, the magnetic field can be represented as

$$\boldsymbol{B_1} = \frac{6\mu_0 \mu_m}{4\pi d^4} z \hat{\boldsymbol{e}}_z, \tag{24a}$$

$$\boldsymbol{B_2} = -\frac{6\mu_0 \mu_m}{4\pi d^4} z \hat{\boldsymbol{e}}_z. \tag{24b}$$

In the same way as the one-NV process, we can get the interaction Hamiltonian of two NV centers, which reads

$$\hat{H}_{int} = \lambda (\hat{a} + \hat{a}^\dagger)(\hat{S}_z^1 - \hat{S}_z^2), \tag{25}$$

where $\lambda = 2\gamma_e B_r a^3 z_0/d^4$ is the coupling strength. Then, the Hamiltonian of the hybrid system is given by

$$\hat{H}_{TT} = \frac{\omega_0}{2}(\hat{\sigma}_z^1 + \hat{\sigma}_z^2) + \omega_{ma}\hat{a}^\dagger \hat{a} + \Lambda(\hat{a} + \hat{a}^\dagger)(\hat{\sigma}_x^1 - \hat{\sigma}_x^2)$$
$$- g_{cu}(\hat{a} + \hat{a}^\dagger)^2 \cos 2\omega_{cu} t. \tag{26}$$

Moving in the rotation frame, the Hamiltonian can be simplified as

$$\hat{H}_{TT} = \frac{\delta_0}{2}(\hat{\sigma}_z^1 + \hat{\sigma}_z^2) + \delta_m \hat{a}^\dagger \hat{a} + \Lambda[\hat{a}(\hat{\sigma}_1^+ - \hat{\sigma}_2^+)$$
$$+ \hat{a}^\dagger (\hat{\sigma}_1^- - \hat{\sigma}_2^-)] - \frac{g_{cu}}{2}(\hat{a}^2 + \hat{a}^{\dagger 2}). \tag{27}$$

In the squeezing frame [i.e., with the Bogoliubov transformation [93,97,100] $\hat{b} = \hat{a} \cosh r - \hat{a}^\dagger \sinh r$ and $\tanh(2r) = g_{cu}/\delta_m$], the Hamiltonian of the hybrid system consisting of the NVs and micromagnet is given by

$$\hat{H}_{RT} = \frac{\delta_0}{2}(\hat{\sigma}_z^1 + \hat{\sigma}_z^2) + \Delta_m \hat{b}^\dagger \hat{b} + \Lambda_{eff}(\hat{b} + \hat{b}^\dagger)(\hat{\sigma}_x^1 - \hat{\sigma}_x^2). \tag{28}$$

With $\delta_0 = 0$, the Hamiltonian can be reduced using the Schrieffer-Wolff transformation [12,107] $\hat{H}_{RT}^{eff} = e^S \hat{H}_{RT} e^{-S}$, where $S = \eta(\hat{b}^\dagger - \hat{b})(\hat{\sigma}_x^1 - \hat{\sigma}_x^2)$ and $\eta = \Lambda_{eff}/\Delta_m$. It is worth noting that the parameter η is much smaller than one, indicating that it satisfies the Lamb-Dicke condition $\eta \ll 1$, which is similar to that for trapped ions [108]. The effective Hamiltonian is given by

$$\hat{H}_{RT}^{eff} = \Delta_m \hat{b}^\dagger \hat{b} - \xi (\hat{\sigma}_x^1 - \hat{\sigma}_x^2)^2, \tag{29}$$

where $\xi = \Lambda_{eff}^2/\Delta_m$. Retaining only the terms containing ξ, we obtain the Ising interaction Hamiltonian

$$\hat{H}_{Ising} = \xi (\hat{\sigma}_x^1 - \hat{\sigma}_x^2)^2, \tag{30}$$

corresponding to the one-axis twisting interaction [109]. In this scenario, the effective spin-spin interaction of the two NVs is obtained, and the phonon is only virtually excited. Figure 5(c) shows the coupling strength between two NVs and the insert depicts the squeezing parameter r as a function of g_{cu}/δ_m. The ratio of the amplified spin-spin coupling ($\xi = \Lambda_{eff}^2/\Delta_m$) to the bare coupling ($\xi_0 = \Lambda^2/\delta_m$), given by $\xi/\xi_0 \propto (e^{2r} \cosh 2r)^2$, exponentially increases. The phonon-mediated spin-spin interaction can be enhanced up to several orders of magnitude stronger than the bare coupling, as the squeezing parameter r increases. It is independent of the specific frame of the phonon since the phonon mode has been adiabatically eliminated. The spin-spin interaction is at the heart of several quantum technologies, such as qubit gates, which are vital for quantum computer implementation. In Sec. IV B, we will consider a two-qubit gate with excellent fidelity and faster gate speed.

IV. APPLICATION

A. Preparing Schrödinger cat states

The single NV hybrid system can be utilized to prepare a Schrödinger cat state [25,110], which is a linear superposition of two coherent states. According to the analysis of Sec. III A, the coupling strength of the NV center and micromagnet has been greatly enhanced, which is critical for preparing a cat state with the spin-mechanical interaction. We assign $\delta_0 = 0$ for the Hamiltonian (17). The Hamiltonian can be diagonalized with the Bogoliubov transformation [93,97,100] $\hat{b} = \hat{a} \cosh r(t) - \hat{a}^{\dagger} \sinh r(t)$ with $\tanh[2r(t)] = g_{cu}(t)/\delta_m$, which reads

$$\hat{H}_{TO} = \hat{H}_{RO} + \hat{H}_{Sq} + \hat{H}_{Err}, \tag{31}$$

$$\hat{H}_{RO} = \Delta_m(t)\hat{b}^{\dagger}\hat{b} + \Lambda_{eff}(t)(\hat{b} + \hat{b}^{\dagger})\hat{\sigma}_x, \tag{32}$$

$$\hat{H}_{Sq} = \frac{\Lambda e^{-r(t)}}{2}(\hat{b} - \hat{b}^{\dagger})(\hat{\sigma}^+ - \hat{\sigma}^-), \tag{33}$$

$$\hat{H}_{Err} = -i\frac{\dot{r}(t)}{2}(\hat{b}^{\dagger 2} - \hat{b}^2), \tag{34}$$

where $\Lambda_{eff}(t) = \Lambda e^{r(t)}/2$ and $\Delta_m(t) = \delta_m/\cosh[2r(t)]$. $\hat{b}$ ($\hat{b}^{\dagger}$) corresponds to the annihilation (creation) operator of the Bogoliubov mode. The Hamiltonian Eq. (32) is the time-dependent Rabi model, and the undesirable corrections are $\hat{H}_{Sq}$ and $\hat{H}_{Err}$. The Hamiltonian $\hat{H}_{Sq}$ can be ignored since it contains $e^{-r(t)}$, as previously stated. We assume that the pump varies slowly over time to maintain adiabaticity during the dynamical process, such that the correction item $\hat{H}_{Err}$ can be ignored because $\dot{r}(t) \approx 0$. Utilizing Magnus expansion [103–106], then, the time evolution operator can be written as $U_{RO}(t) = D[\alpha(t)]\exp[-i\chi(t,0)\hat{b}^{\dagger}\hat{b}]$, where $D[\alpha(t)] = \exp[\alpha(t)\hat{b}^{\dagger} - \alpha^*(t)\hat{b}]\hat{\sigma}_x$ is the displacement operator and $\alpha(t) = -i\Lambda/2\int_0^t \exp[r(t') - i\chi(t,t')]dt'$ is the coherent displacement of phonons in phase space, with $\chi(t,t') = \int_{t'}^t \Delta_m(t'')dt''$. The spin-mechanical system is prepared in the initial state $|\Psi_0\rangle = |0\rangle|\downarrow\rangle$, with $|\downarrow\rangle$ representing the ground state, and the time evolution operator is then applied to the initial state. Finally, we can obtain an entangled cat state

$$\Psi_{final} = \frac{|\alpha(t)\rangle|+\rangle_x - |-\alpha(t)\rangle|-\rangle_x}{\sqrt{2}}, \tag{35}$$

where the states $|\pm\alpha(t)\rangle$ are the phonon mode coherent states, and $|\pm\rangle_x = (|\uparrow\rangle \pm |\downarrow\rangle)/\sqrt{2}$ are the eigenstates of the operator $\hat{\sigma}_x$, with $|\uparrow\rangle$ being the excited state $|e\rangle$. From $t = 0$ to $t = t_f$, the ideal Rabi Hamiltonian Eq. (32) and the total Hamiltonian Eq. (31) are used to carry out the dynamic simulations of the aforementioned process, respectively. If we assume that the initial state is $|0\rangle|\downarrow\rangle$, the spin dephasing is γ_{NV}, and the phonon dissipation is κ_{ma}^S, the dynamic evolution follows the Lindblad master equation

$$\dot{\rho} = -i[\hat{H}_{RO} \text{ or } \hat{H}_{TO}, \hat{\rho}] + \gamma_{NV}D(\hat{\sigma}_z)\hat{\rho} + \kappa_{ma}^S D(\hat{b})\hat{\rho}, \tag{36}$$

where $D(\hat{O})\hat{\rho} = \hat{O}\hat{\rho}\hat{O}^{\dagger} - \{\hat{O}^{\dagger}\hat{O}, \hat{\rho}\}/2$ is the Lindblad operator. Figures 6(a)–6(d) depict the evolution of the phonon-mode Winger function over time using the Hamiltonian $\hat{H}_{RO}$. At the initial time $t = 0$, the squeezed parameter $r(0) = 0$ indicates that the current drive is zero, and the system is
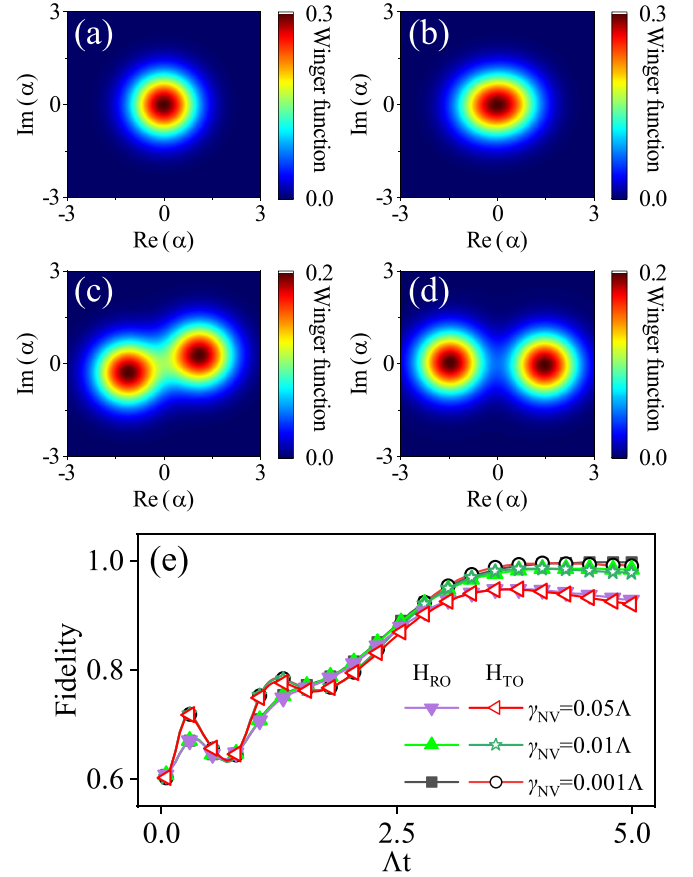

FIG. 6. Schrödinger cat states. With $\kappa_{ma}^S = \gamma_{NV} = 0.01\Lambda$, the Winger functions of the phonon mode are displayed in (a), (b), (c), and (d), corresponding to the situations $\Lambda t = 0$, $\Lambda t = 1.5$, $\Lambda t = 3$, and $\Lambda t = 4.5$, respectively. (e) The fidelity of the cat state is evaluated with different dephasing rates of the NV center. Furthermore, the dynamic process resulting from $\hat{H}_{RO}$ is identical to that resulting from $\hat{H}_{TO}$. Here, $r(t) = r_{max}\tanh(\Lambda t/2)$ where $r_{max} = 1.25$.

prepared in the initial state $|0\rangle|\downarrow\rangle$ [20,94]. The current drive is loaded adiabatically over time, and then the transformed b mode evolves into a well-separated Schrödinger cat state in phase space. In addition, the fidelity of the cat state is depicted in Fig. 6(e) (with the Hamiltonian $\hat{H}_{RO}$), achieving 99.7% when $\gamma_{NV} = 0.001\Lambda$, 98.3% when $\gamma_{NV} = 0.01\Lambda$, and 92.8% when $\gamma_{NV} = 0.05\Lambda$. It is worth noticing that the evolution predicted by $\hat{H}_{RO}$ (solid lines with close symbols) matches that predicted by $\hat{H}_{TO}$ (the solid line with open symbols). It suggests that the unwanted corrections produced by $\hat{H}_{Sq}$ and $\hat{H}_{Err}$ can be ignored.

B. Two-qubit gate

Quantum logic gates [104,111–114] are the core of quantum computation. Geometric quantum computing refers to the quantum computation associated with the pure geometric phase [115]. Based on the different methods of obtaining the geometric phase, the geometric phase gate can be divided into two categories: (i) the conventional geometric phase gate, which acquires the pure geometric phase with adiabatic evolution of qubits, and (ii) the unconventional geometric phase

gate, which acquires the pure geometric phase with the evolution of the Bose mode along a close trajectory in the phase space. Conventional geometric phase gates have been studied with many platforms [115–117]. The two-NV proposal, as discussed in Sec. III C, can be utilized to build an unconventional geometric phase two-qubit gate with high fidelity and faster gate speed. The hybrid system containing two NVs is described by the Hamiltonian (28). As previously discussed, we set $\delta_0 = 0$, and $\hat{b}$ ($\hat{b}^\dagger$) corresponds to the Bogoliubov mode annihilation (creation) operator. Moving in the Bogoliubov-mode interaction frame, we can get

$$\hat{H}_{\mathrm{RT}}^I = \Lambda_{\mathrm{eff}}(\hat{b}e^{-i\Delta_m t} + \hat{b}^\dagger e^{i\Delta_m t})(\hat{\sigma}_x^1 - \hat{\sigma}_x^2). \quad (37)$$

Then, utilizing the Magnus expansion [103–106], the time evolution operator is given by

$$U_{\mathrm{RT}}(t) = D[\alpha(t)]E_{ij}[\zeta(t)], \quad (38)$$

where $D[\alpha(t)] = \exp[\alpha(t)\hat{b}^\dagger - \alpha^*(t)\hat{b}](\hat{\sigma}_x^1 - \hat{\sigma}_x^2)$ denotes the displacement operator, and $\alpha(t) = \Lambda_{\mathrm{eff}}/\Delta_m(1 - e^{i\Delta_m t})$ is the coherent displacement of phonons in phase space. The second item describing spin-spin interaction is given by

$$E_{ij}[\zeta(t)] = \exp\left(\sum_{i,j}^2 \zeta(t)\eta_{ij}\hat{\sigma}_x^i\hat{\sigma}_x^j\right), \quad (39)$$

where

$$\eta_{ij} = \begin{cases} 1, & i = j \\ -1, & i \neq j \end{cases} \quad (40)$$

and $\zeta(t) = i\Lambda_{\mathrm{eff}}^2/\Delta_m^2(\Delta_m t - \sin\Delta_m t)$. The phonon mode returning to its initial state, a gate operation is completed. As a result, the gate time is determined by $\tau = 2\pi/\Delta_m$, at which point the time evolution operator can be represented as

$$U_{\mathrm{RT}}(\tau) = \exp\left(i2\pi\frac{\Lambda_{\mathrm{eff}}^2}{\Delta_m^2}\sum_{i,j}^2\eta_{ij}\hat{\sigma}_x^i\hat{\sigma}_x^j\right). \quad (41)$$

Adjusting the ratio between Λ_{eff} and Δ_m, qubit gates corresponding to different phases can be constructed, such as the $\pi/2$-2-qubit gate described by $U_{\mathrm{RT}}(\tau) = \exp(i\frac{\pi}{8}\sum_{i,j}^2\eta_{ij}\hat{\sigma}_x^i\hat{\sigma}_x^j)$. Supposing that the initial state is the eigenstate of $\hat{\sigma}_x$, then, at time τ, the final state is

$$|+\rangle_x|+\rangle_x \rightarrow |+\rangle_x|+\rangle_x,$$
$$|-\rangle_x|-\rangle_x \rightarrow |-\rangle_x|-\rangle_x,$$
$$|+\rangle_x|-\rangle_x \rightarrow e^{i\pi/2}|+\rangle_x|-\rangle_x,$$
$$|-\rangle_x|+\rangle_x \rightarrow e^{i\pi/2}|-\rangle_x|+\rangle_x. \quad (42)$$

The two-qubit gate only adds a phase to $|+\rangle_x|-\rangle_x$ and $|-\rangle_x|+\rangle_x$, not $|+\rangle_x|+\rangle_x$ and $|-\rangle_x|-\rangle_x$, because the time evolution operator at time τ is $\hat{I}$ when the initial state is the latter. Furthermore, the two-qubit gate is universal, as demonstrated in the literature [118].

Utilizing Eq. (28) for numerical simulations with the dissipation of the phonon mode κ_{ma}^S and the dephasing of NVs γ_{NV}^1 and γ_{NV}^2, the dynamic process can be described by the Lindblad master equation

$$\dot{\hat{\rho}} = -i[\hat{H}_{\mathrm{RT}}, \hat{\rho}] + \kappa_{\mathrm{ma}}^S D(\hat{b})\hat{\rho} + \gamma_{\mathrm{NV}}^1 D(\hat{\sigma}_z^1)\hat{\rho} + \gamma_{\mathrm{NV}}^2 D(\hat{\sigma}_z^2)\hat{\rho},$$
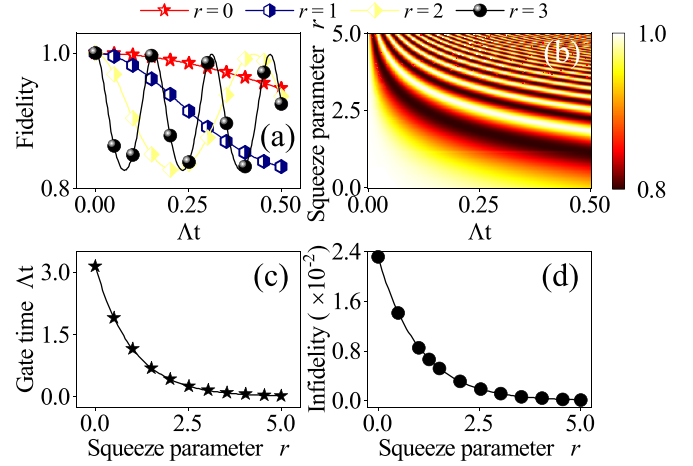$$(43)$$

FIG. 7. (a) and (b) The dynamic process of the two-qubit gate with the varying squeezing parameter r. When the phonon mode evolves back to the original state, a gate operation is accomplished. (c) gate time and (d) infidelity of the two-qubit gate as a function of the squeezing parameter r. The larger the squeezing parameter r, the shorter the gate time and the smaller the gate infidelity. Here, the parameters are $\kappa_{\mathrm{ma}}^S = \gamma_{\mathrm{NV}}^1 = \gamma_{\mathrm{NV}}^2 = 0.01\Lambda$, $\delta_0 = 0$, $\Delta_m = 4\Lambda_{\mathrm{eff}}$ and the initial state is $(|+\rangle_x + |-\rangle_x)/\sqrt{2} \otimes (|+\rangle_x + |-\rangle_x)/\sqrt{2}$.

where $D(\hat{O})\hat{\rho} = \hat{O}\hat{\rho}\hat{O}^\dagger - \{\hat{O}^\dagger\hat{O}, \hat{\rho}\}/2$. As depicted in Figs. 7(a) and 7(b), when the fidelity of the phonon mode reaches its maximum value, a gate operation is finished. It reveals that the two-qubit gate time decreases as the squeezing parameter r increases. Furthermore, Fig. 7(c) indicates that with the squeezing parameter r increasing, the gate time decreases dramatically. The two-qubit-gate infidelity arising from the dephasing of the spins is also affected by the squeezing parameter r shown in Fig. 7(d). It indicates that a two-qubit gate with higher fidelity and shorter gate time can be achieved, with the fidelity being more than 99.9% when the squeezing parameter $r = 3$.

V. EXPERIMENTAL FEASIBILITY

To verify the experimental feasibility of the scheme proposed in this paper, we consider the scheme based on the experimental parameters given in Ref. [52], which include the radius $a = 0.25\,\mu m$, cooling height $h_{\mathrm{cool}} = 3a$, equilibrium position $h_{\mathrm{eq}} = 3a$, equilibrium angle $\phi_{\mathrm{eq}} = 0$ and $\theta_{\mathrm{eq}} = \pi/2$, the density of micromagnet $\rho = 7430\,\mathrm{kg/m^3}$, and residual induction $B_r = 750\,\mathrm{mT}$. Then, the frequency of the oscillator is 347 kHz. According to Ref. [52], the quality factor Q of the oscillator can reach 10^5, and then the dissipation of the mechanical oscillator is assumed to be $\kappa_m/2\pi = \omega_{\mathrm{ma}}/Q \approx 3\,\mathrm{Hz}$ (the damping caused by gas collisions and eddy current is analyzed in Appendix D). The coherence time of NV center can approach 1 s [23,119], and then its dissipation is 1.7 Hz. The coupling strength between the NV center and the micromagnet is 2 kHz with the distance between the NV center and magnetic sphere $d = 2a$, which is consistent with Ref. [52]. Here we take the distance between the NV center and the magnetic sphere as $d = 0.3\,\mu m$, at which point the spin-phonon coupling strength is 17 kHz. A driving current is applied to the hybrid system, with the position $h_{\mathrm{cu}} = 0.3\,\mu m$ and amplitude
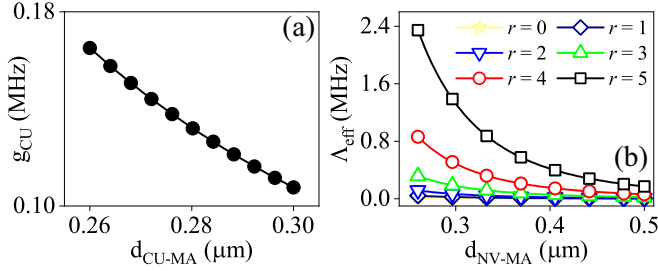
FIG. 8. (a) The coupling strength between the driving current and the micromagnet varies with the distance between them. (b) The coupling strength of the NV and micromagnet grows as the distance between them decreases and the squeezing parameter r increases.

$I_0 = 10$ mA. Figure 8(a) shows the coupling strength between the driving current and the micromagnet as a function of the distance between them d_{CU-MA}. As the distance between them grows, it decreases. Here, the driving strength of the current is taken as $g_{cu}/2\pi = 0.1$ MHz, with $d_{CU-MA} = 0.3$ μm. The coupling strength between the NV center and the micromagnet as a function of the distance between them d_{NV-MA} and the squeezing parameter r is depicted in Fig. 8(b). This shows that the coupling strength can be amplified when decreasing the distance and increasing the squeezing parameter r, reaching 1.3 MHz if $d_{NV-MA} = 0.3$ μm and the squeezing parameter $r = 5$, indicating that it can reach the strong and even ultrastrong regime. To summarize, we can choose appropriate parameters based on the actual experimental conditions. In addition, the proposal is simple to implement under current experimental circumstances.

VI. CONCLUSION

Utilizing NV centers and a levitated micromagnet, we propose a hybrid quantum spin-mechanical system. A time-dependent driving current is applied to the hybrid system, which offers the critical nonlinear resource for the enhancement of the coupling strength. As a result, the spin-phonon and phonon-mediated spin-spin coupling strengths can be enhanced exponentially. The system can be utilized to construct an unconventional two-qubit geometric phase gate with high fidelity and shorter gate time, as well as to prepare Schrödinger cat states with high fidelity. Furthermore, the ground-state cooling approach, which requires the ultrastrong interaction between qubits and oscillators described by Ref. [16], could be more simply implemented with our proposal. In addition, because the trapped frequency is related to the levitated height and the radius of the micromagnet, a wide frequency range can be easily obtained. Our proposal can also be extended to other solid-state spin systems, such as the silicon-vacancy center, germanium-vacancy center, and tin-vacancy center in diamond [20,38,41], allowing for more quantum information processing applications based on quantum levitodynamics.

ACKNOWLEDGMENTS

APPENDIX A: THE MOTION OF THE MECHANICAL OSCILLATOR

In order to solve the oscillation frequency of the micromagnet associated with the three center-of-mass and two orientational degrees of freedom, we need to obtain the motion equation of the micromagnet at the equilibrium position. Utilizing the potential U, the force experienced by the micromagnet is given by

$$f(\boldsymbol{r}) = -\frac{\partial U(\boldsymbol{r})}{\partial \boldsymbol{r}} = -U_s \boldsymbol{J}\frac{\partial u_s(\boldsymbol{u}_s)}{\partial \boldsymbol{u}_s}, \quad (A1)$$

where $\boldsymbol{r} = (x, y, z, \theta, \phi)$, $\boldsymbol{u}_s = \boldsymbol{J} \cdot \boldsymbol{r} = (x/a, y/a, z/a, \theta, \phi)$, and $\boldsymbol{J} = \text{diag}(1/a, 1/a, 1/a, 1, 1)$ with characteristic length scale a. At the equilibrium position, the resultant force on the magnetic sphere is zero, that is, $f(\boldsymbol{u}_{eq}) = 0$. Therefore, the Taylor expansion of the force at the equilibrium position is

$$f^{eq}(\boldsymbol{u}_{eq}) \approx -U_s \boldsymbol{J}^2 \boldsymbol{k}_s \boldsymbol{u}, \quad (A2)$$

where $\boldsymbol{k}_s$ is stiffness matrix whose matrix element is given by

$$k_{ij} = \left.\frac{\partial^2 u_s(\boldsymbol{u})}{\partial u_i \partial u_j}\right|_{\boldsymbol{u}=\boldsymbol{u}_{eq}}. \quad (A3)$$

Then the motion equation of the micromagnet can be written as

$$\ddot{\boldsymbol{u}} + \boldsymbol{W} \cdot \boldsymbol{u} = 0, \quad (A4)$$

where $\boldsymbol{W} = U_s \boldsymbol{J}^2 \mathcal{M}^{-1} \boldsymbol{k}_s$ and $\mathcal{M} = \text{diag}[m, m, m, I_m, I_m]$ is mass matrix, with the mass of the micromagnet $m = \rho 4\pi a^3/3$ and the moment of inertia $I_m = 2ma^2/5$ for spherical rigid body. The eigenfrequency of the system is given by the eigenvalue of $\boldsymbol{W}$, and after simple calculation the matrix $\boldsymbol{W}$ can be reduced to

$$\boldsymbol{W} = \omega_0^2 \boldsymbol{I}_{const} \boldsymbol{k}_s = \omega_0^2 \boldsymbol{k}, \quad (A5)$$

where $\boldsymbol{k} = \boldsymbol{I}_{const} \boldsymbol{k}_s$, $\boldsymbol{I}_{const} = \text{diag}(1, 1, 1, 2.5, 2.5)$, and $\omega_0 = 1/l_s \sqrt{U_s/m}$ with characteristic length scale l_s. Then the oscillation frequency of the micromagnet is $\omega_i = \omega_0 \sqrt{k_i}$, where k_i is the eigenvalue of the matrix $\boldsymbol{k}$ and $i = 1, 2, 3, 4, 5$.

First, we consider that $h_{cool} \to \infty$, that is, there is no trapped flux in the superconductor, such that the potential is given by

$$u_s(\boldsymbol{u}_s; h_{cool} \to \infty, \theta_{cool}, \alpha_s) = \alpha_s x_s + \frac{3 + \cos 2\theta}{6x_s^3}. \quad (A6)$$

Through simple calculation, we can get the minimum value of potential Eq. (A6) at $\theta = \pi/2$ and $x = h_1$, that is, the equilibrium position is $\theta_{eq} = \pi/2$ and $h_{eq} = h_1 = (1/\alpha)^{1/4}$, where h_1 can be obtained by equation $\partial_{x_s} u_s(\boldsymbol{u}_s; h_{cool} \to \infty, \theta_{cool}, \alpha_s) = 0$. In physical units, h_1 is written as

$$h_1 = \left(\frac{a^3 B_r^2}{16\rho g \mu_0}\right)^{\frac{1}{4}}. \quad (A7)$$

Taking advantage of $\theta_{eq} = \pi/2$, $h_{eq} = h_1$, Eq. (A6), and Eq. (A3), the stiffness matrix $\mathbf{k}_s$ is

$$
\mathbf{k}_s = \begin{bmatrix} \frac{4}{h_1^5} & 0 & 0 & 0 & 0 \\ 0 & 0 & 0 & 0 & 0 \\ 0 & 0 & 0 & 0 & 0 \\ 0 & 0 & 0 & \frac{2}{3h_1^2} & 0 \\ 0 & 0 & 0 & 0 & 0 \end{bmatrix}.
\tag{A8}
$$

Utilizing Eq. (A5), we can get $\mathbf{W} = \omega_0^2 \mathbf{k}$ with

$$
\mathbf{k} = \begin{bmatrix} 4 & 0 & 0 & 0 & 0 \\ 0 & 0 & 0 & 0 & 0 \\ 0 & 0 & 0 & 0 & 0 \\ 0 & 0 & 0 & \frac{5h_1^2}{3a} & 0 \\ 0 & 0 & 0 & 0 & 0 \end{bmatrix}
\tag{A9}
$$

and $\omega_0 = [g^4/(a^3 \alpha_{crit})]^{1/8}$. The eigenvalues of matrix $\mathbf{k}$ are $k_1 = 4$, $k_2 = k_3 = k_5 = 0$ and $k_4 = 5h_1^2/(3a)$, and then the eigenfrequency of the micromagnet is given by $\omega_i = \omega_0 \sqrt{k_i}$ with $i = 1, 2, 3, 4, 5$. Of course, the case analyzed above is very ideal. Therefore, we calculate the oscillation frequency of the micromagnet in the presence of the trapped magnetic flux in the following part.

From Fig. 2, we can get the equilibrium $\mathbf{u}_{eq} = (h_{eq}, 0, 0, \pi/2, 0)$. For the convenience of calculation, setting h_1 as the characteristic length scale, we can get

$$
\begin{aligned}
U &= U_s u_s, \\
u_s &= g_u + x_s, \\
g_u &= \frac{3 + \cos 2\theta}{6 x_s^3} - \frac{16}{3} \frac{g_c \cos\theta + g_s \sin\theta}{\left[(x_s + h_{cool})^2 + y_s^2 + z_s^2\right]^{5/2}}, \\
g_c &= -3z_s(x_s + h_{cool}), \\
g_s &= \left[(x_s + h_{cool})^2 + y_s^2 - 2z_s^2\right]\cos\phi - 3z_s y_s \sin\phi,
\end{aligned}
\tag{A10}
$$

with $U_s = mgh_1$ and $\theta_{cool} = \pi/2$. Utilizing the equation $\partial_{z_s} u_s(\mathbf{u}_s; h_{cool}, \pi/2) = 0$, we can get

$$
h_{cool} = h_2 \left[\frac{2}{\left(1 - h_2^4\right)^{1/4}} - 1 \right].
\tag{A11}
$$

The equilibrium position $h_{eq} = h_2$ in the gravity direction is determined by implicit function Eq. (A11). Here, the parameter we considered is $h_2/h_1 \ll 1$, i.e., $h_2 \approx h_{cool}$.

With $\mathbf{u}_s = (h_{eq}, 0, 0, \pi/2, 0)$, Eq. (A10), and Eq. (A3), the stiffness matrix $\mathbf{k}_s$ is

$$
\mathbf{k}_s = \begin{bmatrix} \frac{2}{h_{cool}^5} & 0 & 0 & 0 & 0 \\ 0 & \frac{1}{2h_{cool}^5} & 0 & 0 & 0 \\ 0 & 0 & \frac{3}{2h_{cool}^5} & -\frac{1}{h_{cool}^4} & 0 \\ 0 & 0 & -\frac{1}{h_{cool}^4} & \frac{4}{3h_{cool}^3} & 0 \\ 0 & 0 & 0 & 0 & \frac{2}{3h_{cool}^3} \end{bmatrix}.
\tag{A12}
$$

Utilizing Eq. (A5), we can get $\mathbf{W} = \omega_0^2 \mathbf{k}$ with

$$
\mathbf{k} = \begin{bmatrix} 2 & 0 & 0 & 0 & 0 \\ 0 & \frac{1}{2} & 0 & 0 & 0 \\ 0 & 0 & \frac{3}{2} & -h_{cool} & 0 \\ 0 & 0 & -\frac{5h_{cool}}{2a^2} & \frac{10h_{cool}^2}{3a^2} & 0 \\ 0 & 0 & 0 & 0 & \frac{5h_{cool}^2}{3a^2} \end{bmatrix},
\tag{A13}
$$

where $\omega_0 = B_r a^{-1} \tilde{h}_{cool}^{-5/2}/(4\sqrt{\rho\mu_0})$ in physical units. The eigenvalues of matrix $\mathbf{k}$ are $k_1 = 5\tilde{h}_{cool}^2/3$, $k_2 = 2$, $k_3 = 1/2$, and $k_{4,5} = [9 + 20\tilde{h}_{cool} \pm \sqrt{81 + 400\tilde{h}_{cool}^2}]$ with $\tilde{h}_{cool} = h_{cool}/a$, then the eigenfrequency of the micromagnet is given by $\omega_i = \omega_0 \sqrt{k_i}$, with $i = 1, 2, 3, 4, 5$. We take the parameters radius $a = 0.25 \ \mu$m, mass density $\rho = 7430$ kg/m^3, residual induction $B_r = 750$ mT, cooldown height $h_{cool} = 3a$, and gravity acceleration $g = 9.8$ m/s^2. We can obtain the oscillation frequency of the oscillator as $\omega_x/2\pi = 1903$ kHz, $\omega_y/2\pi = 695$ kHz, and $\omega_z/2\pi = 347$ kHz.

The librational mode of the suspended micromagnet has been studied in Ref. [52], corresponding to the librational frequency $\omega_r = \sqrt{\omega_L \omega_I}$, which precesses around the local magnetic field $\mathbf{B}_{loc}$ with Einstein–de Haas frequency $\omega_I = \rho_s V/(I_m \gamma_e)$ due to the conservation of angular momentum, where ρ_s is the spin density, the local magnetic field $\mathbf{B}_{loc}$ is the sum of the magnetic field generated by superconductivity and the external magnetic field, and ω_L is the Larmor frequency. Here, the spin density is taken as $\rho_s = B_r/(\gamma_e \mu_B)$, then the Einstein–de Haas frequency frequency is $\omega_I/2\pi = 9.01$ kHz. The frequency of rotation mode is $\omega_r/2\pi = 1588$ kHz with the local magnetic field $|\mathbf{B}_{loc}| = 10$ mT and the Larmor frequency $\omega_L/2\pi = 280$ MHz.

APPENDIX B: INTERACTION BETWEEN MICROMAGNET AND NV

1. Translational modes

As shown in Fig. 1, the position vector of the magnetic sphere is $\mathbf{r}_l = (x, y, z)$. Note that here we consider three directions of simple harmonic oscillation. The magnetic moment of the micromagnet is $\boldsymbol{\mu}_l = \mu_m(0, 0, 1)$ along the z direction. The position coordinate of the NV center is $(h_{eq}, 0, d)$. According to Eq. (1), the magnetic field induced by the micromagnet at the position of the NV center is

$$
\begin{aligned}
B_x &= \frac{\mu_0 \mu_m}{4\pi} \frac{3}{r^5}(d - z)(h_{eq} - x), \\
B_y &= \frac{\mu_0 \mu_m}{4\pi} \frac{3}{r^5}(d - z)(-y), \\
B_z &= \frac{\mu_0 \mu_m}{4\pi}\left[\frac{3}{r^5}(d - z)(d - z) - \frac{1}{r^3}\right],
\end{aligned}
\tag{B1}
$$

where $r = \sqrt{(x - h_{eq})^2 + y^2 + (z - d)^2}$. According to the results in Eq. (B1), we know that the magnetic field at the NV color center is mainly in the z direction, and the magnetic field in the xy direction is almost zero, so we only consider the magnetic field in the z direction. Then the Hamiltonian for the interaction between NV and the magnetic sphere is

$$
\hat{H}_{int} = \gamma_e B_z S_z.
\tag{B2}
$$

Expanding the magnetic field B_z at the equilibrium position $(x_{eq}, y_{eq}, z_{eq}) = (h_{eq}, 0, 0)$ yields (removing the constant and higher-order terms)

$$B_z = \left.\partial_x B_z\right|_{\boldsymbol{u}_{eq}=(h_{eq},0,0)} x + \left.\partial_y B_z\right|_{\boldsymbol{u}_{eq}=(h_{eq},0,0)} y$$
$$+ \left.\partial_z B_z\right|_{\boldsymbol{u}_{eq}=(h_{eq},0,0)} z. \tag{B3}$$

After calculation we can get $\left.\partial_x B_z\right|_{x=h_{eq}} = 0$, $\left.\partial_y B_z\right|_{y=0} = 0$, and $\left.\partial_z B_z\right|_{z=0} = \mu_0 \mu_m/(4\pi)(6/d^4)$. Then the interaction Hamiltonian $\hat{H}_{int}$ can be reduced to

$$\hat{H}_{int} = \lambda(\hat{a} + \hat{a}^\dagger)S_z, \tag{B4}$$

with $\lambda = \gamma_e \frac{\mu_0 \mu_m}{4\pi} \frac{6}{d^4} z_0$, that is, the simple harmonic oscillation in the xy direction is not coupled with the NV center.

2. Rotation mode

In this section, the coupling strength between the rotation mode (precession) and the NV center is estimated. Considering the rotation mode alone, the coordinate and magnetic moment of the micromagnet can be written as $(h_{eq}, 0, 0)$ and $\boldsymbol{B}_l = \mu_m(\cos\theta, \sin\phi\sin\theta, \cos\phi\sin\theta)$, respectively. The coordinate of the NV center is $(h_{eq}, 0, d)$, and the distance between NV and the magnetic sphere is d. According to Eq. (1), the magnetic field experienced by the NV center, generated by the magnetic sphere, is given by

$$B_x = -\frac{\mu_0 \mu_m}{4\pi} \frac{1}{r^3} \cos\theta,$$
$$B_y = -\frac{\mu_0 \mu_m}{4\pi} \frac{1}{r^3} \sin\phi\sin\theta,$$
$$B_z = \frac{\mu_0 \mu_m}{4\pi} \left(\frac{3d^2}{r^5} - \frac{1}{r^3}\right) \cos\phi\sin\theta. \tag{B5}$$

Since the rotation mode is a precession near the equilibrium position (precess around the local magnetic field, i.e., around the z axis), we have $\delta\theta = \pi/2 - \theta \to 0$ and $\phi \to 0$. Then Eq. (B5) can be reduced to

$$B_x = \frac{\mu_0 \mu_m}{4\pi} \frac{1}{d^3} \delta\theta,$$
$$B_y = -\frac{\mu_0 \mu_m}{4\pi} \frac{1}{d^3} \phi,$$
$$B_z = \frac{\mu_0 \mu_m}{4\pi} \frac{1}{d^3} (\phi^2 + \delta\theta^2). \tag{B6}$$

According to the interaction Hamiltonian $\hat{H}_{int}^{RN} = \gamma_e \boldsymbol{B} \cdot \hat{\boldsymbol{S}} = \lambda_{RN}^x \hat{S}_x + \lambda_{RN}^y \hat{S}_y + \lambda_{RN}^z \hat{S}_z$, the coupling strength of the rotation mode and the NV center can be estimated from $\lambda_{RN}^x = \gamma_e \mu_0 \mu_m/(4\pi d^3)\delta\theta_{zpf}$, $\lambda_{RN}^y = \gamma_e \mu_0 \mu_m/(4\pi d^3)\phi_{zpf}$ and $\lambda_{RN}^z = \gamma_e \mu_0 \mu_m/(4\pi d^3)(\phi_{zpf}^2 + \delta\theta_{zpf}^2)/2$ with $\delta\theta_{zpf} = \phi_{zpf} = \sqrt{\hbar/(2I_m\omega_r)}$ [35].

Here, we take the parameters $a = 0.25~\mu m$, $d = 0.3~\mu m$, and $B_r = 750$ mT, so that the coupling strengths are $\lambda/2\pi = 17$ kHz, $\lambda_{RN}^x/2\pi = 2.62$ kHz, $\lambda_{RN}^y/2\pi = 2.62$ kHz, and $\lambda_{RN}^z/2\pi = 1.72$ mHz. According to the previous analysis, we know that the oscillation frequency in the z direction and the frequency of the rotation mode are $\omega_z/2\pi = 347$ kHz and $\omega_r/2\pi = 1588$ kHz, respectively, with parameters $a = 0.25~\mu m$, mass density $\rho = 7430$ kg/m³, residual induction

$B_r = 750$ mT, cooldown height $h_{cool} = 3a$, and gravity acceleration $g = 9.8$ m/s². We consider here the coupling between the NV center and the micromagnet translational mode, and the resonance of the NV center and the translational mode is achieved by microwave driving of the NV center using the method of dressed states; however, in this case the big detuning condition is satisfied between the NV center and the rotating mode. Therefore, there is no energy exchange between the rotating mode and NV center due to big detuning. Besides, the coupling strength of the NV center and rotation mode is approximately satisfied much less than that of the NV center and translational mode, i.e., the former can be ignored.

APPENDIX C: THE HAMILTONIAN OF DRIVE CURRENT

Current pumping $I_{cu}(t) = I_0 \cos(2\omega_{cu}t)$ is added to the hybrid system to enhance coupling strength. The position of the origin current and image current in the zx plane are $\boldsymbol{R}_{or} = (h_{cu}, 0, 0)$ and $\boldsymbol{R}_{im} = (-h_{cu}, 0, 0)$, respectively. When just the magnetic field in the z direction near the equilibrium position is considered, the total magnetic field created by the origin and image current is given by

$$\boldsymbol{B}_{cu} = \boldsymbol{B}_{or} + \boldsymbol{B}_{im} = \frac{\mu_0 I}{2\pi}\left(\frac{1}{r_{or}} + \frac{1}{r_{im}}\right)\hat{\boldsymbol{e}}_z. \tag{C1}$$

Then the potential energy of the micromagnet in the magnetic field generated by the current can be written as

$$U_{cu} = -\boldsymbol{\mu} \cdot \boldsymbol{B}_{cu}, \tag{C2a}$$
$$= -\frac{\mu_0 \mu_m I}{2\pi}\left[\frac{1}{\sqrt{(h_{eq} - h_{cu})^2 + z^2}}\right]$$
$$- \frac{\mu_0 \mu_m I}{2\pi}\left[\frac{1}{\sqrt{(h_{eq} + h_{cu})^2 + z^2}}\right]. \tag{C2b}$$

By expanding at the equilibrium position, dropping constant items and high-order terms, the potential energy can be represented as

$$U_{cu} = -\frac{1}{2}k_{cu}\hat{z}^2\cos(2\omega_{cu}t), \tag{C3}$$

where

$$k_{cu} = \frac{\mu_0 \mu_m I_0}{2\pi}\left[\frac{1}{(h_{cu} - h_{eq})^3} + \frac{1}{(h_{cu} + h_{eq})^3}\right]. \tag{C4}$$

Quantizing the potential energy, the Hamiltonian is given by

$$\hat{H}_{cu} = -g_{cu}(\hat{a} + \hat{a}^\dagger)^2 \cos(2\omega_{cu}t), \tag{C5}$$

where $g_{cu} = k_{cu}z_0^2/2$ is the coupling strength between the drive current and the micromagnet.

Next we consider the effect of the magnetic field generated by the current on the NV center. The positions of the NV center, current, and micromagnet are $(h_{eq}, 0, d)$, $(h_{cu}, 0, 0)$, and $(h_{eq}, 0, 0)$, respectively, with $d = 0.3~\mu m$, $h_{cu} = 0.55~\mu m$, and $h_{eq} = 3a$. The magnetic field generated by the current at

the position of the NV center can be written as

$$B_x^{\mathrm{CU-NV}} = \frac{\mu_0 I_0}{2\pi\sqrt{2}d_{\mathrm{CU-NV}}},$$

$$B_z^{\mathrm{CU-NV}} = \frac{\mu_0 I_0}{2\pi\sqrt{2}d_{\mathrm{CU-NV}}}, \quad \text{(C6)}$$

with the distance of current to NV center $d_{\mathrm{CU-NV}} = \sqrt{(h_{\mathrm{cu}} - h_{\mathrm{eq}})^2 + d^2}$. Using Eq. (C6), the magnetic field generated by the current at the NV color center can be obtained: $B_x^{\mathrm{CU-NV}} = B_z^{\mathrm{CU-NV}} = 3$ mT. According to Eq. (B1), we can calculate the magnetic field generated by the micromagnet at the position of the NV center: $B_z = 289$ mT, i.e., $B_z^{\mathrm{CU-NV}} \ll B_z$. We can neglect the effect of the magnetic field in the z direction of the current on the NV center. For the magnetic field in the x direction generated by the current at the position of the NV center, we can take the bias magnetic field $B_0 \gg B_x^{\mathrm{CU-NV}}$ of the NV center, so we can also ignore the effect of $B_x^{\mathrm{CU-NV}}$ on the NV spin. In summary, the effect of the magnetic field generated by the current on the NV center is negligible.

APPENDIX D: THE DAMPING RATE

In this section the calculations are mainly performed for the eddy-current damping and gas-collision damping [52,120,121].

1. The eddy-current damping

For the convenience of considering the eddy-current damping, we equate the micromagnet to a current ring. The motion of the micromagnet in the plane parallel to the superconducting surface will not bring a change of magnetic flux. In this case there will be no damping from the image dipole, which is always rotating or moving with the micromagnet. However, the rotation or translation of the micromagnet in the plane perpendicular to the superconducting surface brings about a change in the magnetic flux, and in this case there is a damping of the eddy current to the micromagnet. It means that eddy-current damping impedes motion perpendicular to the superconducting surface, but not parallel to the superconducting surface.

First of all, we study the rotation perpendicular to the superconducting surface. Assuming that the rotation frequency of the current loop is ω_θ, the voltage induced by the change in magnetic flux is [120]

$$U_\theta = \frac{d\Phi_\theta}{dt} = \frac{d[B_z A \cos\theta(t)]}{dt} = B_z A \omega_\theta \cos[\theta(t)], \quad \text{(D1)}$$

with the area of the current ring A. The resistance of the micromagnet is given by $R = 2/(\sigma a)$. The energy lost in each cycle is

$$E_d^\theta = \int_0^T \frac{U_\theta^2}{R} dt = \frac{\pi^3 B_z^2 a^4 \omega_\theta}{R}. \quad \text{(D2)}$$

The total energy stored can be written as

$$E_\theta = \frac{1}{2} I_m \omega_\theta^2. \quad \text{(D3)}$$

Then the Q_r factor is given by

$$Q_r = 2\pi \frac{E_\theta}{E_d^\theta} = \frac{16\rho\omega_\theta}{15\pi\sigma B_z^2}. \quad \text{(D4)}$$

We can obtain the damping rate

$$\frac{\gamma_\theta}{2\pi} = \frac{\omega_\theta}{Q_\theta} = \frac{15\pi\sigma B_z^2}{16\rho}. \quad \text{(D5)}$$

Next we calculate the damping of the translational mode perpendicular to the superconducting surface. Setting the oscillation frequency as ω_x, the voltage induced by the change of magnetic flux is

$$U_x = \frac{d\Phi_x}{dt} = \frac{d[\delta B_z A \sin\omega_x t]}{dt} = \delta B_z A \omega_\theta \sin\omega_x t, \quad \text{(D6)}$$

where δB_z is the change in the magnetic field at the center of the ring during the oscillation and we assume that the magnitude of the magnetic field penetrating the ring is equal to the magnetic field at the center of the ring, which results in a larger calculated damping rate than the actual damping rate.

The energy lost in each cycle is

$$E_d^x = \int_0^T \frac{U_x^2}{R} dt = \frac{\pi^3 \delta B_z^2 a^4 \omega_x}{R}. \quad \text{(D7)}$$

The total energy stored can be given by

$$E_x = \frac{1}{2} m \omega_x^2 x_{zpf}^2. \quad \text{(D8)}$$

Then the Q_x factor is given by

$$Q_x = 2\pi \frac{E_x}{E_d^x} = \frac{8\rho\omega_x x_{zpf}^2}{3\pi \delta B_z^2 a^2 \sigma}. \quad \text{(D9)}$$

We can obtain the damping rate

$$\frac{\gamma_x}{2\pi} = \frac{\omega_x}{Q_x} = \frac{3\pi \delta B_z^2 a^2 \sigma}{8\rho x_{zpf}^2}. \quad \text{(D10)}$$

According to $\boldsymbol{B}_{\mathrm{eff}} = \boldsymbol{B}_f + 1/2\boldsymbol{B}_i$, the magnetic field in each direction at the equilibrium position $(x_{\mathrm{eq}}, y_{\mathrm{eq}}, z_{\mathrm{eq}}, \theta_{\mathrm{eq}}, \phi_{\mathrm{eq}}) = (h_{\mathrm{eq}}, 0, 0, \pi/2, 0)$ can be written as

$$B_x = 0,$$
$$B_y = 0,$$
$$B_z = \frac{\mu_0 \mu_m}{4\pi}\left(\frac{1}{r_f^3} - \frac{1}{r_i^3}\right). \quad \text{(D11)}$$

Then we can get $B_z = 0.57$ mT and $\delta B_z = 0.52$ mT. We take the parameters: radius of micromagnet $a = 0.25$ μm, resistance of the micromagnet $\sigma = 10^7$ $\Omega^{-1}\mathrm{m}^{-1}$ [120], oscillation frequency in the x direction $\omega_x/2\pi = 1903$ kHz, and zero-point fluctuation in the x direction $x_{zpf} = \sqrt{\hbar/(2m\omega_x)}$ to calculate the damping rate, $\gamma_\theta/2\pi = 0.13$ mHz and $\gamma_x/2\pi = 0.03$ mHz. That is, the damping due to the eddy-current is much smaller than the dissipation assumed in the main text.

2. The gas-collision damping

The higher the vacuum level of the experimental environment, the smaller the damping due to the collision of residual air molecules with suspended particles. The damping rate caused by the gas molecules is given by [52,65,122–124]

$$\frac{\gamma_{\text{gas}}}{2\pi} = \frac{3\eta_g a}{m} \frac{0.619}{K_n + 0.619}\left(1 + \frac{0.31K_n}{K_n^2 + 1.152K_n + 0.785}\right),$$

(D12)

where Knudsen number $K_n = \bar{\lambda}/a$ and gas viscosity coefficient $\eta_g = nm_g\sqrt{8k_BT_g/(\pi m_g)}\bar{\lambda}/2$ with number density $n = P_g/(k_BT_g)$, gas pressure P_g, gas temperature T_g, average mass of each gas molecule m_g, free mean path of gas molecules $\bar{\lambda} = k_BT_g/(\sqrt{2}P_g s)$, collision cross section $s = \pi d_g^2$, gas molecular diameter d_g, and Boltzmann constant k_B. Here we take the parameters gas temperature $T_g = 10$ mK and gas molecular diameter $d_g = 0.372$ nm. Then the damping rate due to gas collisions is $\gamma_{\text{gas}}/2\pi = 0.15$ Hz at parameter $P_g = 10^{-5}$ mBar.

[1] Z.-L. Xiang, S. Ashhab, J. Q. You, and F. Nori, Hybrid quantum circuits: Superconducting circuits interacting with other quantum systems, Rev. Mod. Phys. **85**, 623 (2013).

[2] A. A. Clerk, K. W. Lehnert, P. Bertet, J. R. Petta, and Y. Nakamura, Hybrid quantum systems with circuit quantum electrodynamics, Nat. Phys. **16**, 257 (2020).

[3] M. Wallquist, K. Hammerer, P. Rabl, M. Lukin, and P. Zoller, Hybrid quantum devices and quantum engineering, Phys. Scr. **2009**, 014001 (2009).

[4] H. Walther, B. T. H. Varcoe, B.-G. Englert, and T. Becker, Cavity quantum electrodynamics, Rep. Prog. Phys. **69**, 1325 (2006).

[5] A. Blais, A. L. Grimsmo, S. M. Girvin, and A. Wallraff, Circuit quantum electrodynamics, Rev. Mod. Phys. **93**, 025005 (2021).

[6] W. Qin, A. Miranowicz, G. Long, J. Q. You, and F. Nori, Proposal to test quantum wave-particle superposition on massive mechanical resonators, npj Quantum Inf. **5**, 58 (2019).

[7] P. Huillery, T. Delord, L. Nicolas, M. Van Den Bossche, M. Perdriat, and G. Hétet, Spin mechanics with levitating ferromagnetic particles, Phys. Rev. B **101**, 134415 (2020).

[8] X.-L. Dong, P.-B. Li, T. Liu, and F. Nori, Unconventional Quantum Sound-Matter Interactions in Spin-Optomechanical-Crystal Hybrid Systems, Phys. Rev. Lett. **126**, 203601 (2021).

[9] O. Arcizet, V. Jacques, A. Siria, P. Poncharal, P. Vincent, and S. Seidelin, A single nitrogen-vacancy defect coupled to a nanomechanical oscillator, Nat. Phys. **7**, 879 (2011).

[10] S. Hong, M. S. Grinolds, P. Maletinsky, R. L. Walsworth, M. D. Lukin, and A. Yacoby, Coherent, mechanical control of a single electronic spin, Nano. Lett. **12**, 3920 (2012).

[11] S. Kolkowitz, A. C. B. Jayich, Q. P. Unterreithmeier, S. D. Bennett, P. Rabl, J. G. E. Harris, and M. D. Lukin, Coherent sensing of a mechanical resonator with a single-spin qubit, Science **335**, 1603 (2012).

[12] I. Wilson-Rae, P. Zoller, and A. Imamoḡlu, Laser Cooling of a Nanomechanical Resonator Mode to its Quantum Ground State, Phys. Rev. Lett. **92**, 075507 (2004).

[13] P.-B. Li, Y.-C. Liu, S.-Y. Gao, Z.-L. Xiang, P. Rabl, Y.-F. Xiao, and F.-L. Li, Hybrid Quantum Device Based on *NV* Centers in Diamond Nanomechanical Resonators Plus Superconducting Waveguide Cavities, Phys. Rev. Appl. **4**, 044003 (2015).

[14] S. D. Bennett, N. Y. Yao, J. Otterbach, P. Zoller, P. Rabl, and M. D. Lukin, Phonon-Induced Spin-Spin Interactions in Diamond Nanostructures: Application to Spin Squeezing, Phys. Rev. Lett. **110**, 156402 (2013).

[15] K. V. Kepesidis, S. D. Bennett, S. Portolan, M. D. Lukin, and P. Rabl, Phonon cooling and lasing with nitrogen-vacancy centers in diamond, Phys. Rev. B **88**, 064105 (2013).

[16] K. Streltsov, J. S. Pedernales, and M. B. Plenio, Ground-State Cooling of Levitated Magnets in Low-Frequency Traps, Phys. Rev. Lett. **126**, 193602 (2021).

[17] P. Rabl, P. Cappellaro, M. V. G. Dutt, L. Jiang, J. R. Maze, and M. D. Lukin, Strong magnetic coupling between an electronic spin qubit and a mechanical resonator, Phys. Rev. B **79**, 041302(R) (2009).

[18] Z. Y. Xu, Y. M. Hu, W. L. Yang, M. Feng, and J. F. Du, Deterministically entangling distant nitrogen-vacancy centers by a nanomechanical cantilever, Phys. Rev. A **80**, 022335 (2009).

[19] L.-g. Zhou, L. F. Wei, M. Gao, and X.-b. Wang, Strong coupling between two distant electronic spins via a nanomechanical resonator, Phys. Rev. A **81**, 042323 (2010).

[20] P.-B. Li, Y. Zhou, W.-B. Gao, and F. Nori, Enhancing Spin-Phonon and Spin-Spin Interactions Using Linear Resources in a Hybrid Quantum System, Phys. Rev. Lett. **125**, 153602 (2020).

[21] L. Chotorlishvili, D. Sander, A. Sukhov, V. Dugaev, V. R. Vieira, A. Komnik, and J. Berakdar, Entanglement between nitrogen vacancy spins in diamond controlled by a nanomechanical resonator, Phys. Rev. B **88**, 085201 (2013).

[22] P. Rabl, S. J. Kolkowitz, F. H. L. Koppens, J. G. E. Harris, P. Zoller, and M. D. Lukin, A quantum spin transducer based on nanoelectromechanical resonator arrays, Nat. Phys. **6**, 602 (2010).

[23] P. Ovartchaiyapong, K. W. Lee, B. A. Myers, and A. C. B. Jayich, Dynamic strain-mediated coupling of a single diamond spin to a mechanical resonator, Nat. Commun. **5**, 4429 (2014).

[24] J. Teissier, A. Barfuss, P. Appel, E. Neu, and P. Maletinsky, Strain Coupling of a Nitrogen-Vacancy Center Spin to a Diamond Mechanical Oscillator, Phys. Rev. Lett. **113**, 020503 (2014).

[25] M. Asjad and D. Vitali, Reservoir engineering of a mechanical resonator: Generating a macroscopic superposition state and monitoring its decoherence, J. Phys. B: At. Mol. Opt. Phys. **47**, 045502 (2014).

[26] C. Sánchez Muñoz, A. Lara, J. Puebla, and F. Nori, Hybrid Systems for the Generation of Nonclassical Mechanical States via Quadratic Interactions, Phys. Rev. Lett. **121**, 123604 (2018).

[27] E. R. MacQuarrie, T. A. Gosavi, N. R. Jungwirth, S. A. Bhave, and G. D. Fuchs, Mechanical Spin Control of Nitrogen-

Vacancy Centers in Diamond, Phys. Rev. Lett. **111**, 227602 (2013).

[28] B. Pigeau, S. Rohr, L. Mercier de Lépinay, A. Gloppe, V. Jacques, and O. Arcizet, Observation of a phononic Mollow triplet in a multimode hybrid spin-nanomechanical system, Nat. Commun. **6**, 8603 (2015).

[29] S. G. Carter, A. S. Bracker, G. W. Bryant, M. Kim, C. S. Kim, M. K. Zalalutdinov, M. K. Yakes, C. Czarnocki, J. Casara, M. Scheibner, and D. Gammon, Spin-Mechanical Coupling of an InAs Quantum Dot Embedded in a Mechanical Resonator, Phys. Rev. Lett. **121**, 246801 (2018).

[30] P.-B. Li, Z.-L. Xiang, P. Rabl, and F. Nori, Hybrid Quantum Device with Nitrogen-Vacancy Centers in Diamond Coupled to Carbon Nanotubes, Phys. Rev. Lett. **117**, 015502 (2016).

[31] P. K. Shandilya, D. P. Lake, M. J. Mitchell, D. D. Sukachev, and P. E. Barclay, Optomechanical interface between telecom photons and spin quantum memory, Nat. Phys. **17**, 1420 (2021).

[32] A. Lemmer, A. Bermudez, and M. B. Plenio, Driven geometric phase gates with trapped ions, New J. Phys. **15**, 083001 (2013).

[33] D. Porras and J. I. Cirac, Effective Quantum Spin Systems with Trapped Ions, Phys. Rev. Lett. **92**, 207901 (2004).

[34] J. W. Britton, B. C. Sawyer, A. C. Keith, C. C. J. Wang, J. K. Freericks, H. Uys, M. J. Biercuk, and J. J. Bollinger, Engineered two-dimensional Ising interactions in a trapped-ion quantum simulator with hundreds of spins, Nature (London) **484**, 489 (2012).

[35] T. Delord, L. Nicolas, Y. Chassagneux, and G. Hétet, Strong coupling between a single nitrogen-vacancy spin and the rotational mode of diamonds levitating in an ion trap, Phys. Rev. A **96**, 063810 (2017).

[36] J. F. Barry, J. M. Schloss, E. Bauch, M. J. Turner, C. A. Hart, L. M. Pham, and R. L. Walsworth, Sensitivity optimization for NV-diamond magnetometry, Rev. Mod. Phys. **92**, 015004 (2020).

[37] M. W. Doherty, N. B. Manson, P. Delaney, F. Jelezko, J. Wrachtrup, and L. C. Hollenberg, The nitrogen-vacancy colour centre in diamond, Phys. Rep. **528**, 1 (2013).

[38] C. Bradac, W. Gao, J. Forneris, M. E. Trusheim, and I. Aharonovich, Quantum nanophotonics with group IV defects in diamond, Nat. Commun. **10**, 5625 (2019).

[39] S. Meesala, Y.-I. Sohn, B. Pingault, L. Shao, H. A. Atikian, J. Holzgrafe, M. Gündoğan, C. Stavrakas, A. Sipahigil, C. Chia, R. Evans, M. J. Burek, M. Zhang, L. Wu, J. L. Pacheco, J. Abraham, E. Bielejec, M. D. Lukin, M. Atatüre, and M. Lončar, Strain engineering of the silicon-vacancy center in diamond, Phys. Rev. B **97**, 205444 (2018).

[40] M.-A. Lemonde, S. Meesala, A. Sipahigil, M. J. A. Schuetz, M. D. Lukin, M. Loncar, and P. Rabl, Phonon Networks with Silicon-Vacancy Centers in Diamond Waveguides, Phys. Rev. Lett. **120**, 213603 (2018).

[41] C. Hepp, T. Müller, V. Waselowski, J. N. Becker, B. Pingault, H. Sternschulte, D. Steinmüller-Nethl, A. Gali, J. R. Maze, M. Atatüre, and C. Becher, Electronic Structure of the Silicon Vacancy Color Center in Diamond, Phys. Rev. Lett. **112**, 036405 (2014).

[42] J.-Q. Chen, Y.-F. Qiao, X.-L. Dong, X.-L. Hei, and P.-B. Li, Dissipation-assisted preparation of steady spin-squeezed states of SiV centers, Phys. Rev. A **103**, 013709 (2021).

[43] A. K. Singh, L. Chotorlishvili, S. Srivastava, I. Tralle, Z. Toklikishvili, J. Berakdar, and S. K. Mishra, Generation of coherence in an exactly solvable nonlinear nanomechanical system, Phys. Rev. B **101**, 104311 (2020).

[44] J. Prat-Camps, C. Teo, C. C. Rusconi, W. Wieczorek, and O. Romero-Isart, Ultrasensitive Inertial and Force Sensors with Diamagnetically Levitated Magnets, Phys. Rev. Appl. **8**, 034002 (2017).

[45] C. Timberlake, G. Gasbarri, A. Vinante, A. Setter, and H. Ulbricht, Acceleration sensing with magnetically levitated oscillators above a superconductor, Appl. Phys. Lett. **115**, 224101 (2019).

[46] A. Vinante, P. Falferi, G. Gasbarri, A. Setter, C. Timberlake, and H. Ulbricht, Ultralow Mechanical Damping with Meissner-Levitated Ferromagnetic Microparticles, Phys. Rev. Appl. **13**, 064027 (2020).

[47] B. R. Slezak, C. W. Lewandowski, J.-F. Hsu, and B. D'Urso, Cooling the motion of a silica microsphere in a magneto-gravitational trap in ultra-high vacuum, New J. Phys. **20**, 063028 (2018).

[48] C. Navau, S. Minniberger, M. Trupke, and A. Sanchez, Levitation of superconducting microrings for quantum magnetomechanics, Phys. Rev. B **103**, 174436 (2021).

[49] C. C. Rusconi, V. Pöchhacker, J. I. Cirac, and O. Romero-Isart, Linear stability analysis of a levitated nanomagnet in a static magnetic field: Quantum spin stabilized magnetic levitation, Phys. Rev. B **96**, 134419 (2017).

[50] L. S. Walker, G. R. M. Robb, and A. J. Daley, Measurement and feedback for cooling heavy levitated particles in low-frequency traps, Phys. Rev. A **100**, 063819 (2019).

[51] Y. Leng, R. Li, X. Kong, H. Xie, D. Zheng, P. Yin, F. Xiong, T. Wu, C.-K. Duan, Y. Du, Z.-q. Yin, P. Huang, and J. Du, Mechanical Dissipation Below 1μHz with a Cryogenic Diamagnetic Levitated Micro-Oscillator, Phys. Rev. Appl. **15**, 024061 (2021).

[52] J. Gieseler, A. Kabcenell, E. Rosenfeld, J. D. Schaefer, A. Safira, M. J. A. Schuetz, C. Gonzalez-Ballestero, C. C. Rusconi, O. Romero-Isart, and M. D. Lukin, Single-Spin Magnetomechanics with Levitated Micromagnets, Phys. Rev. Lett. **124**, 163604 (2020).

[53] F. Xiong, T. Wu, Y. Leng, R. Li, C.-K. Duan, X. Kong, P. Huang, Z. Li, Y. Gao, X. Rong, and J. Du, Searching spin-mass interaction using a diamagnetic levitated magnetic-resonance force sensor, Phys. Rev. Res. **3**, 013205 (2021).

[54] M. T. Johnsson, G. K. Brennen, and J. Twamley, Macroscopic superpositions and gravimetry with quantum magnetomechanics, Sci. Rep. **6**, 37495 (2016).

[55] C. C. Rusconi, M. J. A. Schuetz, J. Gieseler, M. D. Lukin, and O. Romero-Isart, Hybrid architecture for engineering magnonic quantum networks, Phys. Rev. A **100**, 022343 (2019).

[56] L. Martinetz, K. Hornberger, J. Millen, M. S. Kim, and B. A. Stickler, Quantum electromechanics with levitated nanoparticles, npj Quantum Inf. **6**, 101 (2020).

[57] O. Romero-Isart, L. Clemente, C. Navau, A. Sanchez, and J. I. Cirac, Quantum Magnetomechanics with Levitating Superconducting Microspheres, Phys. Rev. Lett. **109**, 147205 (2012).

[58] T. Delord, P. Huillery, L. Nicolas, and G. Hétet, Spin-cooling of the motion of a trapped diamond, Nature (London) **580**, 56 (2020).

[59] C. C. Rusconi, M. Perdriat, G. Hétet, O. Romero-Isart, and B. A. Stickler, Spin-Controlled Quantum Interference of Levitated Nanorotors, Phys. Rev. Lett. **129**, 093605 (2022).

[60] O. Gunawan, J. Kristiano, and H. Kwee, Magnetic-tip trap system, Phys. Rev. Res. **2**, 013359 (2020).

[61] M. C. O'Brien, S. Dunn, J. E. Downes, and J. Twamley, Magneto-mechanical trapping of micro-diamonds at low pressures, Appl. Phys. Lett. **114**, 053103 (2019).

[62] J.-F. Hsu, P. Ji, C. W. Lewandowski, and B. D'Urso, Cooling the motion of diamond nanocrystals in a magneto-gravitational trap in high vacuum, Sci. Rep. **6**, 30125 (2016).

[63] Z.-q. Yin, T. Li, X. Zhang, and L. M. Duan, Large quantum superpositions of a levitated nanodiamond through spin-optomechanical coupling, Phys. Rev. A **88**, 033614 (2013).

[64] U. Delić, M. Reisenbauer, K. Dare, D. Grass, V. Vuletić, N. Kiesel, and M. Aspelmeyer, Cooling of a levitated nanoparticle to the motional quantum ground state, Science **367**, 892 (2020).

[65] T. Li, S. Kheifets, and M. G. Raizen, Millikelvin cooling of an optically trapped microsphere in vacuum, Nat. Phys. **7**, 527 (2011).

[66] F. Tebbenjohanns, M. Frimmer, V. Jain, D. Windey, and L. Novotny, Motional Sideband Asymmetry of a Nanoparticle Optically Levitated in Free Space, Phys. Rev. Lett. **124**, 013603 (2020).

[67] J. Millen, T. S. Monteiro, R. Pettit, and A. N. Vamivakas, Optomechanics with levitated particles, Rep. Prog. Phys. **83**, 026401 (2020).

[68] M. G. Latorre, J. Hofer, M. Rudolph, and W. Wieczorek, Chip-based superconducting traps for levitation of micrometer-sized particles in the Meissner state, Supercond. Sci. Technol. **33**, 105002 (2020).

[69] Z. Yang, T. Johansen, H. Bratsberg, G. Helgesen, and A. Skjeltorp, Vibrations of a magnet levitated over a flat superconductor, Physica C: Superconductivity **160**, 461 (1989).

[70] Y. Ma, T. M. Hoang, M. Gong, T. Li, and Z.-q. Yin, Proposal for quantum many-body simulation and torsional matter-wave interferometry with a levitated nanodiamond, Phys. Rev. A **96**, 023827 (2017).

[71] J. Millen and B. A. Stickler, Quantum experiments with microscale particles, Contemp. Phys. **61**, 155 (2020).

[72] M. Perdriat, C. Pellet-Mary, P. Huillery, L. Rondin, and G. Hétet, Spin-mechanics with nitrogen-vacancy centers and trapped particles, Micromachines **12**, 651 (2021).

[73] M. Cirio, G. K. Brennen, and J. Twamley, Quantum Magnetomechanics: Ultrahigh-Q-Levitated Mechanical Oscillators, Phys. Rev. Lett. **109**, 147206 (2012).

[74] H. Pino, J. Prat-Camps, K. Sinha, B. P. Venkatesh, and O. Romero-Isart, On-chip quantum interference of a superconducting microsphere, Quant. Sci. Techn. **3**, 025001 (2018).

[75] B. A. Stickler, K. Hornberger, and M. S. Kim, Quantum rotations of nanoparticles, Nat. Rev. Phys. **3**, 589 (2021).

[76] C. Gonzalez-Ballestero, M. Aspelmeyer, L. Novotny, R. Quidant, and O. Romero-Isart, Levitodynamics: Levitation and control of microscopic objects in vacuum, Science **374**, eabg3027 (2021).

[77] J. Bourhill, N. Kostylev, M. Goryachev, D. L. Creedon, and M. E. Tobar, Ultrahigh cooperativity interactions between magnons and resonant photons in a YIG sphere, Phys. Rev. B **93**, 144420 (2016).

[78] C. Gonzalez-Ballestero, D. Hümmer, J. Gieseler, and O. Romero-Isart, Theory of quantum acoustomagnonics and acoustomechanics with a micromagnet, Phys. Rev. B **101**, 125404 (2020).

[79] Y. Tabuchi, S. Ishino, T. Ishikawa, R. Yamazaki, K. Usami, and Y. Nakamura, Hybridizing Ferromagnetic Magnons and Microwave Photons in the Quantum Limit, Phys. Rev. Lett. **113**, 083603 (2014).

[80] C. Gonzalez-Ballestero, J. Gieseler, and O. Romero-Isart, Quantum Acoustomechanics with a Micromagnet, Phys. Rev. Lett. **124**, 093602 (2020).

[81] O. O. Soykal and M. E. Flatté, Strong Field Interactions between a Nanomagnet and a Photonic Cavity, Phys. Rev. Lett. **104**, 077202 (2010).

[82] N. J. Lambert, J. A. Haigh, and A. J. Ferguson, Identification of spin wave modes in yttrium iron garnet strongly coupled to a co-axial cavity, J. Appl. Phys. **117**, 053910 (2015).

[83] N. Kostylev, M. Goryachev, and M. E. Tobar, Superstrong coupling of a microwave cavity to yttrium iron garnet magnons, Appl. Phys. Lett. **108**, 062402 (2016).

[84] X. Zhang, C.-L. Zou, L. Jiang, and H. X. Tang, Strongly Coupled Magnons and Cavity Microwave Photons, Phys. Rev. Lett. **113**, 156401 (2014).

[85] Y.-P. Wang, G.-Q. Zhang, D. Zhang, T.-F. Li, C.-M. Hu, and J. Q. You, Bistability of Cavity Magnon Polaritons, Phys. Rev. Lett. **120**, 057202 (2018).

[86] X.-L. Hei, X.-L. Dong, J.-Q. Chen, C.-P. Shen, Y.-F. Qiao, and P.-B. Li, Enhancing spin-photon coupling with a micromagnet, Phys. Rev. A **103**, 043706 (2021).

[87] W. Xiong, M. Tian, G.-Q. Zhang, and J. Q. You, Strong long-range spin-spin coupling via a Kerr magnon interface, Phys. Rev. B **105**, 245310 (2022).

[88] M. Kaczor, I. Tralle, P. Jakubczyk, S. Stagraczyński, and L. Chotorlishvili, Switching of the information backflow between a helical spin system and non-Markovian bath, Ann. Phys. **442**, 168918 (2022).

[89] W. Qin, A. Miranowicz, P.-B. Li, X.-Y. Lü, J. Q. You, and F. Nori, Exponentially Enhanced Light-Matter Interaction, Cooperativities, and Steady-State Entanglement Using Parametric Amplification, Phys. Rev. Lett. **120**, 093601 (2018).

[90] P. Groszkowski, H.-K. Lau, C. Leroux, L. C. G. Govia, and A. A. Clerk, Heisenberg-Limited Spin Squeezing via Bosonic Parametric Driving, Phys. Rev. Lett. **125**, 203601 (2020).

[91] X.-Y. Lü, Y. Wu, J. R. Johansson, H. Jing, J. Zhang, and F. Nori, Squeezed Optomechanics with Phase-Matched Amplification and Dissipation, Phys. Rev. Lett. **114**, 093602 (2015).

[92] P.-B. Li, H.-R. Li, and F.-L. Li, Enhanced electromechanical coupling of a nanomechanical resonator to coupled superconducting cavities, Sci. Rep. **6**, 19065 (2016).

[93] M.-A. Lemonde, N. Didier, and A. A. Clerk, Enhanced nonlinear interactions in quantum optomechanics via mechanical amplification, Nat. Commun. **7**, 11338 (2016).

[94] C. Leroux, L. C. G. Govia, and A. A. Clerk, Enhancing Cavity Quantum Electrodynamics via Antisqueezing: Synthetic Ultrastrong Coupling, Phys. Rev. Lett. **120**, 093602 (2018).

[95] W. Ge, B. C. Sawyer, J. W. Britton, K. Jacobs, J. J. Bollinger, and M. Foss-Feig, Trapped Ion Quantum Information Processing with Squeezed Phonons, Phys. Rev. Lett. **122**, 030501 (2019).

[96] W. Ge, B. C. Sawyer, J. W. Britton, K. Jacobs, M. Foss-Feig, and J. J. Bollinger, Stroboscopic approach to trapped-ion quantum information processing with squeezed phonons, Phys. Rev. A **100**, 043417 (2019).

[97] S. C. Burd, R. Srinivas, H. M. Knaack, W. Ge, A. C. Wilson, D. J. Wineland, D. Leibfried, J. J. Bollinger, D. T. C. Allcock, and D. H. Slichter, Quantum amplification of boson-mediated interactions, Nat. Phys. **17**, 898 (2021).

[98] D. Rugar and P. Grütter, Mechanical Parametric Amplification and Thermomechanical Noise Squeezing, Phys. Rev. Lett. **67**, 699 (1991).

[99] A. A. Kordyuk, Magnetic levitation for hard superconductors, J. Appl. Phys. **83**, 610 (1998).

[100] S. C. Burd, R. Srinivas, J. J. Bollinger, A. C. Wilson, D. J. Wineland, D. Leibfried, D. H. Slichter, and D. T. C. Allcock, Quantum amplification of mechanical oscillator motion, Science **364**, 1163 (2019).

[101] J.-M. Pirkkalainen, E. Damskägg, M. Brandt, F. Massel, and M. A. Sillanpää, Squeezing of Quantum Noise of Motion in a Micromechanical Resonator, Phys. Rev. Lett. **115**, 243601 (2015).

[102] E. E. Wollman, C. U. Lei, A. J. Weinstein, J. Suh, A. Kronwald, F. Marquardt, A. A. Clerk, and K. C. Schwab, Quantum squeezing of motion in a mechanical resonator, Science **349**, 952 (2015).

[103] S.-L. Zhu, C. Monroe, and L.-M. Duan, Arbitrary-speed quantum gates within large ion crystals through minimum control of laser beams, Europhys. Lett. **73**, 485 (2006).

[104] C. F. Roos, Ion trap quantum gates with amplitude-modulated laser beams, New J. Phys. **10**, 013002 (2008).

[105] A. Arnal, F. Casas, and C. Chiralt, A general formula for the Magnus expansion in terms of iterated integrals of right-nested commutators, J. Phys. Commun. **2**, 035024 (2018).

[106] S. Blanes, F. Casas, J. Oteo, and J. Ros, The Magnus expansion and some of its applications, Phys. Rep. **470**, 151 (2009).

[107] A. Albrecht, A. Retzker, F. Jelezko, and M. B. Plenio, Coupling of nitrogen vacancy centres in nanodiamonds by means of phonons, New J. Phys. **15**, 083014 (2013).

[108] H. Wang and I. Lekavicius, Coupling spins to nanomechanical resonators: Toward quantum spin-mechanics, Appl. Phys. Lett. **117**, 230501 (2020).

[109] M. Kitagawa and M. Ueda, Squeezed spin states, Phys. Rev. A **47**, 5138 (1993).

[110] M. Das, J. K. Verma, and P. K. Pathak, Generation of the superposition of mesoscopic states of a nanomechanical resonator by a single two-level system, Phys. Rev. A **96**, 033837 (2017).

[111] X.-Y. Chen and Z.-q. Yin, Universal quantum gates between nitrogen-vacancy centers in a levitated nanodiamond, Phys. Rev. A **99**, 022319 (2019).

[112] P. H. Leung, K. A. Landsman, C. Figgatt, N. M. Linke, C. Monroe, and K. R. Brown, Robust 2-Qubit Gates in a Linear Ion Crystal Using a Frequency-Modulated Driving Force, Phys. Rev. Lett. **120**, 020501 (2018).

[113] P. J. Lee, K.-A. Brickman, L. Deslauriers, P. C. Haljan, L.-M. Duan, and C. Monroe, Phase control of trapped ion quantum gates, J. Opt. B: Quantum Semiclass. Opt. **7**, S371 (2005).

[114] D. Leibfried, B. DeMarco, V. Meyer, D. Lucas, M. Barrett, J. Britton, W. M. Itano, B. Jelenković, C. Langer, T. Rosenband, and D. J. Wineland, Experimental demonstration of a robust, high-fidelity geometric two ion-qubit phase gate, Nature (London) **422**, 412 (2003).

[115] G. Falci, R. Fazio, G. M. Palma, J. Siewert, and V. Vedral, Detection of geometric phases in superconducting nanocircuits, Nature (London) **407**, 355 (2000).

[116] J. A. Jones, V. Vedral, A. Ekert, and G. Castagnoli, Geometric quantum computation using nuclear magnetic resonance, Nature (London) **403**, 869 (2000).

[117] L.-M. Duan, J. I. Cirac, and P. Zoller, Geometric manipulation of trapped ions for quantum computation, Science **292**, 1695 (2001).

[118] D. E. Deutsch, A. Barenco, and A. Ekert, Universality in quantum computation, Proc. R. Soc. Lond. **449**, 669 (1995).

[119] N. Bar-Gill, L. M. Pham, A. Jarmola, D. Budker, and R. L. Walsworth, Solid-state electronic spin coherence time approaching one second, Nat. Commun. **4**, 1743 (2013).

[120] T. Wang, S. Lourette, S. R. O'Kelley, M. Kayci, Y. B. Band, D. F. J. Kimball, A. O. Sushkov, and D. Budker, Dynamics of a Ferromagnetic Particle Levitated over a Superconductor, Phys. Rev. Appl. **11**, 044041 (2019).

[121] A. Vinante, C. Timberlake, and H. Ulbricht, Levitated micromagnets in superconducting traps: A new platform for tabletop fundamental physics experiments, Entropy **24**, 1642 (2022).

[122] S. A. Beresnev, V. G. Chernyak, and G. A. Fomyagin, Motion of a spherical particle in a rarefied gas. Part 2. Drag and thermal polarization, J. Fluid Mech. **219**, 405 (1990).

[123] T. Li, S. Kheifets, D. Medellin, and M. G. Raizen, Measurement of the instantaneous velocity of a Brownian particle, Science **328**, 1673 (2010).

[124] T. Li and M. G. Raizen, Brownian motion at short time scales, Ann. Phys. **525**, 281 (2013).